Title
The glyoxal budget and its contribution to organic aerosol for Los Angeles, California, during CalNex 2010

Journal
Journal of Geophysical Research Atmospheres, 116(20)

ISSN
0148-0227

Authors
Washenfelder, RA
Young, CJ
Brown, SS
et al.

Publication Date
2011

DOI
10.1029/2011JD016314

The glyoxal budget and its contribution to organic aerosol for Los Angeles, California, during CalNex 2010

R. A. Washenfelder,[1,2] C. J. Young,[1,2] S. S. Brown,[2] W. M. Angevine,[1,2] E. L. Atlas,[3] D. R. Blake,[4] D. M. Bon,[1,2] M. J. Cubison,[1,5] J. A. de Gouw,[1,2] S. Dusanter,[6,7,8] J. Flynn,[9] J. B. Gilman,[1,2] M. Graus,[1,2] S. Griffith,[6] N. Grossberg,[9] P. L. Hayes,[1,5] J. L. Jimenez,[1,5] W. C. Kuster,[1,2] B. L. Lefer,[9] I. B. Pollack,[1,2] T. B. Ryerson,[2] H. Stark,[1,10] P. S. Stevens,[6] and M. K. Trainer[2]

Received 3 June 2011; revised 11 August 2011; accepted 12 August 2011; published 28 October 2011.

[1] Recent laboratory and field studies have indicated that glyoxal is a potentially large contributor to secondary organic aerosol mass. We present in situ glyoxal measurements acquired with a recently developed, high sensitivity spectroscopic instrument during the CalNex 2010 field campaign in Pasadena, California. We use three methods to quantify the production and loss of glyoxal in Los Angeles and its contribution to organic aerosol. First, we calculate the difference between steady state sources and sinks of glyoxal at the Pasadena site, assuming that the remainder is available for aerosol uptake. Second, we use the Master Chemical Mechanism to construct a two-dimensional model for gas-phase glyoxal chemistry in Los Angeles, assuming that the difference between the modeled and measured glyoxal concentration is available for aerosol uptake. Third, we examine the nighttime loss of glyoxal in the absence of its photochemical sources and sinks. Using these methods we constrain the glyoxal loss to aerosol to be 0–5 × 10^{-5} s^{-1} during clear days and (1 ± 0.3) × 10^{-5} s^{-1} at night. Between 07:00–15:00 local time, the diurnally averaged secondary organic aerosol mass increases from 3.2 μg m^{-3} to a maximum of 8.8 μg m^{-3}. The constraints on the glyoxal budget from this analysis indicate that it contributes 0–0.2 μg m^{-3} or 0–4% of the secondary organic aerosol mass.

Citation: Washenfelder, R. A., et al. (2011), The glyoxal budget and its contribution to organic aerosol for Los Angeles, California, during CalNex 2010, *J. Geophys. Res.*, *116*, D00V02, doi:10.1029/2011JD016314.

1. Introduction

[2] Atmospheric aerosol particles cause negative human health effects, reduce visibility, and alter the Earth's radiative budget. Organic compounds make up a large part of fine particulate mass, accounting for 20–90% of aerosol mass in the lower troposphere [*Kanakidou et al.*, 2005; *Zhang et al.*, 2007]. This material is composed of primary organic aerosol (POA) which is directly emitted, and secondary organic aerosol (SOA) which is formed from gas-phase oxidation products. SOA mass is typically greater than POA mass in both urban and rural areas [*Zhang et al.*, 2007]. Although the formation and evolution of SOA are important in understanding the total atmospheric aerosol budget, they are poorly characterized.

[3] A temperature-dependent equilibrium model based on vapor pressure is the conventional method to describe the gas/particle partitioning of organic compounds [*Pankow*, 1994a, 1994b]. However, the effect of heterogeneous reactions and the condensation of some smaller, volatile compounds have typically not been included in conventional partitioning-based models [*Kroll and Seinfeld*, 2005]. For field measurements, such conventional models underpredict organic aerosol mass in polluted air, both in the boundary layer and aloft [*de Gouw et al.*, 2005; *Heald et al.*, 2005; *Johnson et al.*, 2006; *Volkamer et al.*, 2006b]. More recent parameterizations predict SOA concentrations in better agreement with observations [*Robinson et al.*, 2007; *Dzepina et al.*, 2009; *Jimenez et al.*, 2009], but uncertainty

[1]Cooperative Institute for Research in Environmental Sciences, University of Colorado at Boulder, Boulder, Colorado, USA.
[2]Chemical Sciences Division, Earth System Research Laboratory, National Oceanic and Atmospheric Administration, Boulder, Colorado, USA.
[3]Division of Marine and Atmospheric Chemistry, University of Miami, Miami, Florida, USA.
[4]Department of Chemistry, University of California, Irvine, California, USA.
[5]Department of Chemistry and Biochemistry, University of Colorado at Boulder, Boulder, USA.
[6]Center for Research in Environmental Science, School of Public and Environmental Affairs and Department of Chemistry, Indiana University, Bloomington, Indiana, USA.
[7]Université Lille Nord de France, Lille, France.
[8]EMDouai, Douai, France.
[9]Department of Earth and Atmospheric Sciences, University of Houston, Houston, Texas, USA.
[10]Aerodyne Research, Incorporated, Billerica, Massachusetts, USA.

0148-0227/11/2011JD016314

remains for both the precursors and the physical and chemical processes [*Dzepina et al.*, 2011].

[4] Glyoxal is the simplest alpha-dicarbonyl, with chemical structure HC(O)C(O)H, and is one of the most prevalent dicarbonyls in the ambient atmosphere. Glyoxal is formed from the photooxidation of ethyne, ethene, aromatic hydrocarbons, isoprene, and monoterpenes [*Fu et al.*, 2008]. Laboratory studies have shown that glyoxal contributes to SOA mass, despite having a relatively high vapor pressure that would preclude its condensation in the conventional gas/particle partitioning model. Glyoxal has been detected directly in atmospheric cloud, fog, and dew water samples [*Steinberg et al.*, 1985; *Igawa et al.*, 1989]. In aqueous solutions representative of clouds and fog, laboratory experiments have shown a link between glyoxal processing and SOA through the production of organic acids and larger oligomeric compounds [*Hastings et al.*, 2005; *Carlton et al.*, 2007; *Shapiro et al.*, 2009; *Tan et al.*, 2009]. Glyoxal uptake has been observed for both inorganic aerosol [*Jang et al.*, 2002; *Kroll et al.*, 2005; *Liggio et al.*, 2005a, 2005b; *Corrigan et al.*, 2008; *Galloway et al.*, 2009; *Volkamer et al.*, 2009] and aerosol containing organic or amino acids [*Corrigan et al.*, 2008]. Chamber studies using ammonium sulfate seed aerosol have shown that from 1.6% [*Jang and Kamens*, 2001] to 3–5% [*Kroll et al.*, 2005] of glyoxal partitions into the aerosol phase.

[5] These laboratory studies have indicated that glyoxal uptake onto inorganic aerosol may depend on aerosol acidity [*Jang et al.*, 2002; *Liggio et al.*, 2005a, 2005b; *Corrigan et al.*, 2008] (although this result was contradicted by *Kroll et al.* [2005]), relative humidity [*Hastings et al.*, 2005; *Corrigan et al.*, 2008], or aerosol ionic strength [*Kroll et al.*, 2005]. More recent work combines these ideas about relative humidity and acidity, arguing that the liquid water content of inorganic aerosol is the important parameter [*Volkamer et al.*, 2009].

[6] Published studies have reported conflicting results regarding the reversibility of glyoxal uptake. The reversibility may depend on the chemical reactions that occur within the bulk aqueous aerosol, and vary by aerosol composition. Product studies have shown that heterogeneous reactions of glyoxal can yield more complex products than hydrated monomers, dimers, and oligomers [*De Haan et al.*, 2009a, 2009b; *Galloway et al.*, 2009]. If glyoxal uptake is reversible, then an effective Henry's Law constant can be defined to include both dissolution and additional reversible heterogeneous reactions. The effective Henry's Law constant for glyoxal uptake to deliquesced ammonium sulfate is 2.6×10^7 M atm^{-1} [*Kroll et al.*, 2005], and varies with aerosol composition [*Corrigan et al.*, 2008; *Ip et al.*, 2009]. In addition to the aerosol uptake into inorganic and organic aerosol described above, two recent chamber studies have observed that uptake occurs more rapidly under irradiated conditions than dark conditions [*Galloway et al.*, 2009; *Volkamer et al.*, 2009]. In each case, the authors observed that these processes were irreversible. A detailed model framework for the reported glyoxal processing by aerosols has been developed by *Ervens and Volkamer* [2010].

[7] Recent advances in analytical techniques to measure glyoxal in ambient air have provided new data to test atmospheric models of its production, loss, and potential contribution to SOA. Historically, glyoxal was collected in solution for later analysis by high-performance liquid chromatography or gas chromatography [*Fung and Grosjean*, 1981; *Spaulding et al.*, 2002]. In the past decade, differential optical absorption spectroscopy (DOAS) [*Volkamer et al.*, 2005a], multiaxis differential optical absorption spectroscopy (Max-DOAS) [*Sinreich et al.*, 2007], cavity enhanced absorption spectroscopy (CEAS) [*Washenfelder et al.*, 2008], laser induced phosphorescence [*Huisman et al.*, 2008], and cavity enhanced - differential optical absorption spectroscopy (CE-DOAS) [*Thalman and Volkamer*, 2010] have been demonstrated for rapid measurement of glyoxal at ambient concentrations.

[8] A detailed analysis of glyoxal's contribution to SOA in an urban area was performed for the 2003 Mexico City Metropolitan Area Field Campaign (MCMA-2003) [*Volkamer et al.*, 2007]. DOAS was used in Mexico City to detect glyoxal by its structured absorption in the 420–465 nm spectral region [*Volkamer et al.*, 2005a]. *Volkamer et al.* [2007] constructed a budget using the Master Chemical Mechanism (MCM) and demonstrated that 70–95% of glyoxal loss could be attributed to aerosol uptake. Different mechanisms for heterogeneous glyoxal uptake onto aerosols were examined. Based on these results, production and loss of glyoxal alone explained more than 15% of the observed SOA mass in Mexico City [*Volkamer et al.*, 2007; *Dzepina et al.*, 2009].

[9] During summer 2010, the CalNex field campaign in Southern California included a large number of chemical and aerosol measurements from ship, aircraft, and ground-based platforms. One of the primary goals of the CalNex study was to understand aerosol formation in an urban environment. The city of Los Angeles is the second largest in the United States, with over 12 million residents in the greater urban area [*U.S. Census Bureau*, 2006]. Although Los Angeles is an industrialized city with significant anthropogenic emissions, it represents an important contrast to Mexico City, where emission controls for volatile organic compounds (VOCs) lag those that have been implemented in California.

[10] We deployed a new glyoxal field instrument at the CalNex ground site in Pasadena, California. This instrument is based on CEAS [*Washenfelder et al.*, 2008]. In addition to glyoxal, the Pasadena ground site contained instruments for VOCs, OH, O_3, CO, CO_2, nitrogen oxides, aerosol size distribution, aerosol chemical composition, photolysis, meteorology, and other trace gas and aerosol measurements. The combination of these measurements, together with ship-based measurements upwind and aircraft-based measurements throughout the boundary layer, allow a detailed analysis of chemical sources, sinks, and transport within the Los Angeles basin. This study provides a very detailed field data set for quantitatively understanding the glyoxal budget. In this paper, we present three separate methods for quantifying glyoxal contribution to aerosol mass.

2. Experiment

2.1. Overview of the CalNex Field Site in Pasadena, California

[11] The CalNex 2010 ground site was located at the California Institute of Technology campus in Pasadena, California (34.140582 N, 118.122455 W, 236 m above

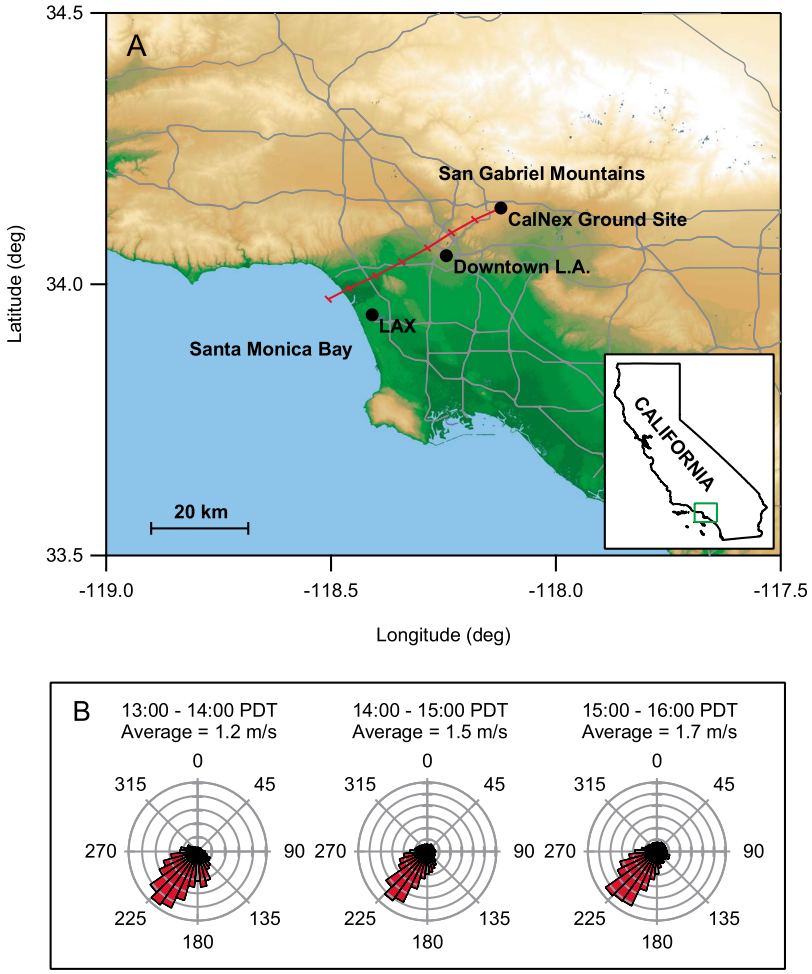

Figure 1. (a) Map of southern California, indicating the location of the Pasadena ground site, downtown Los Angeles, and Los Angeles International Airport (LAX). The average WRF back trajectory for 16:00 PDT for the eight clear, fog-free days described in the text (red line with ticks indicating 30 min elapsed time) shows daytime wind direction from the southwest and an average transport time of 3.25 h from the coast. (b) Measured wind directions and average wind speeds at the CalNex ground site, grouped by one-hour periods from 13:00–16:00 PDT, indicating steady southwest wind.

mean sea level). Measurements were conducted between 15 May and 15 June 2010. Figure 1a shows the location of the Pasadena ground site within the greater Los Angeles area. The site is located within the San Gabriel Valley, 7 km south of the San Gabriel Mountains and 18 km northeast of downtown Los Angeles. The site falls within the dense urban area of Los Angeles County, with extensive mobile and industrial emission sources. Both anthropogenic and biogenic sources are located in the vicinity of the field site, including oak and eucalyptus trees which are efficient isoprene emitters [*Guenther et al.*, 1994]. Satellite images of vegetation indicate additional likely upwind biogenic sources of isoprene. The prevailing wind direction during daytime in Pasadena is onshore flow, as plotted in the wind roses in Figure 1b. Southwesterly winds during the day bring air masses from the Santa Monica Bay through central Los Angeles to Pasadena.

2.2. IBBCEAS Field Instrument for CHOCHO and NO_2

[12] During the CalNex campaign, CHOCHO, NO_2, and HONO were simultaneously measured using a newly constructed field instrument, consisting of three independent optical cavities. The first is a cavity ring-down spectroscopy (CRDS) channel at 403 nm for NO_2, following the work of *Fuchs et al.* [2009]. The second and third cavities are incoherent broadband cavity enhanced absorption spectroscopy (IBBCEAS) channels at 354–388 nm for HONO and NO_2 and 438–472 nm for CHOCHO and NO_2. The IBBCEAS channels are conceptually similar to the laboratory instrument described previously by our group [*Washenfelder et al.*, 2008], with a number of operational improvements.

[13] Briefly, the 438–472 nm IBBCEAS channel consists of an LED light source, collimating lens, optical cavity, collection optics, band-pass filter, optical fiber bundle, and grating spectrometer with CCD detector. During the CalNex field campaign, the optical system, including LED, optical cavity, and inlet, was mounted on the top of a 10-m tower in a temperature-controlled, waterproof enclosure. The grating spectrometer, mass flow controllers, and some electronics were installed in a trailer with optical fibers, signal cables, and power cables to the optical system. This arrangement

Table 1. Relevant Measurements Acquired at the Pasadena Ground Site During CalNex 2010

Species	Technique	Uncertainty (1σ)[a]	Frequency	Reference
Glyoxal	IBBCEAS	±(40 pptv + 15%)	1 min	This work
Speciated VOCs	Gas chromatography – mass spectrometry (GC-MS)	5–25% (hydrocarbons) 20–35% (oxygenates)	30 min	[*Gilman et al.*, 2010]
O_3	UV differential absorption	±(0.4 ppbv + 4%)	1 min	Thermo Scientific model 49c
OH	Laser Induced Fluorescence (LIF-FAGE)	±(4×10^5 cm^{-3} + 18%)	15 min	[*Dusanter et al.*, 2009]
NO	Chemiluminescence	±4%	1 min	Thermo Scientific model 42i-TL
NO_2	Conversion to NO; chemiluminescence	±6%	1 min	Thermo Scientific model 42i-TL BLC
Photolysis	Scanning Actinic Flux Spectroradiometer (SAFS)	±30%	1 min	[*Shetter and Muller*, 1999]
Particle number distribution	Scanning mobility particle sizer (SMPS)	Size: ±5% Concentration: ±15%	5 min	TSI Inc. model 3936
Organic Aerosol Mass	High-Resolution Aerosol Mass Spectrometer (AMS)	±30%	2.5 min	Aerodyne Research HR-ToF-AMS; [*DeCarlo et al.*, 2006]

[a]For uncertainties given as ±(x pptv + y%), x represents the precision and y represents the accuracy.

allowed the inlet to be as short as possible, to minimize potential sampling losses. The sample air was filtered to remove aerosol, which would limit the effective path length and reduce the sensitivity to CHOCHO and NO_2. Sampling artifacts were minimized by using an automated filter changer [*Dube et al.*, 2006] with Teflon membrane filters, which were replaced every 90 min. Comparison of NO_2, CHOCHO, and HONO concentrations before and after filter changes showed no evidence for production or loss. Mirror reflectivity (or cavity loss) was calculated using the method described by *Washenfelder et al.* [2008] from the known Rayleigh scattering extinctions of helium and zero air. Spectra of helium or dry zero air (N_2 + O_2) were measured at regular intervals by introducing a flow to the inlet that exceeded the total sample flow to completely fill the sample cells with either gas.

[14] Spectra were integrated for 0.45 s. During post-processing, spectra were averaged for 1 min periods. Zero air spectra were acquired for 1.5 min once every 5 min, while helium spectra were acquired for 2 min once every 30 min. To characterize the noise of the detector, background spectra were acquired under dark conditions once every 2 h. The pixel-dependent dark signal was then scaled to the integrated time and subtracted from the sample spectra. The cavity extinction as a function of wavelength, $\alpha(\lambda)$, was calculated following the method of *Washenfelder et al.* [2008] using interpolated zero air spectra. For spectral fitting, reference spectra for NO_2 [*Vandaele et al.*, 1998] and CHOCHO [*Volkamer et al.*, 2005b] were convolved with a Gaussian line shape with full width at half maximum of 0.56 nm, corresponding to the measured instrument line shape at 455 nm. DOASIS spectral fitting software [*Kraus*, 2006] was used to retrieve number densities of CHOCHO and NO_2. The 2-σ precision of the glyoxal retrievals in ambient air was 80 pptv in 1 min and 25 pptv in 10 min, as determined from the variability at low glyoxal concentrations during short nighttime periods. This is worse than the 2-σ precision of 58 pptv in 1 min reported for laboratory measurements of glyoxal in dry zero air [*Washenfelder et al.*, 2008]. The glyoxal measurements were validated in the field by standard additions from a pure glyoxal sample maintained at −78°C. The glyoxal concentrations in the standard additions were measured by the CRDS instrument at 403 nm. Due to difficulties with the temperature control of the optical system early in the campaign, the best and most continuous data from the IBBCEAS instrument were acquired from 29 May to 15 June 2010.

2.3. Chemistry, Aerosol, and Meteorological Measurements at the CalNex Ground Site

[15] For the CalNex ground site measurements used in this analysis, Table 1 summarizes the instrumental techniques, uncertainty, sampling frequency, and provides references with further details. The stated uncertainty in Table 1 includes both precision and accuracy. Speciated VOCs were reported for 5 min out of every 30 min using gas chromatography-mass spectrometry (GC-MS) [*Gilman et al.*, 2010]. These included C_2–C_{10} alkanes, C_2–C_5 alkenes, ethyne, C_6–C_9 aromatics, C_2–C_5 aldehydes, aromatics, isoprene, methyl vinyl ketone (MVK), methacrolein, and α-pinene. Other chemical measurements included OH at 15 min time resolution [*Dusanter et al.*, 2009] and O_3 at 1 min time resolution. Aerosol number distribution was measured in 50 size bins between 7–690 nm using a TSI Scanning Mobility Particle Sizer (SMPS). Bulk submicron aerosol composition was reported using a High-Resolution Aerosol Mass Spectrometer (AMS) [*DeCarlo et al.*, 2006]. Measurements of NO, NO_x, NO_y, CO, and CO_2 were used qualitatively to understand air quality and flow patterns during the field campaign.

[16] The CalNex Pasadena ground site was equipped with a meteorological station with temperature/RH sensor (Campbell Scientific Inc., HMP35C), a barometric pressure transducer (Vaisala, PTA-427) and a wind monitor (R. M. Young, 05103). The anemometer was mounted on an aluminum rod extending 2.5 m above the top platform of the trace gas tower, with the temperature/RH sensor located 0.5 m below the anemometer. All meteorological data were logged at 1 Hz. Photolysis rates were calculated from solar spectra acquired using a scanning actinic flux spectroradiometer [*Shetter and Muller*, 1999]. Boundary layer height was measured by a ceilometer (Vaisala, CL31) [*Munkel et al.*, 2007].

2.4. Additional Data Sets

[17] The ground site was part of the larger CalNex field campaign that included the NOAA WP-3D aircraft, Woods

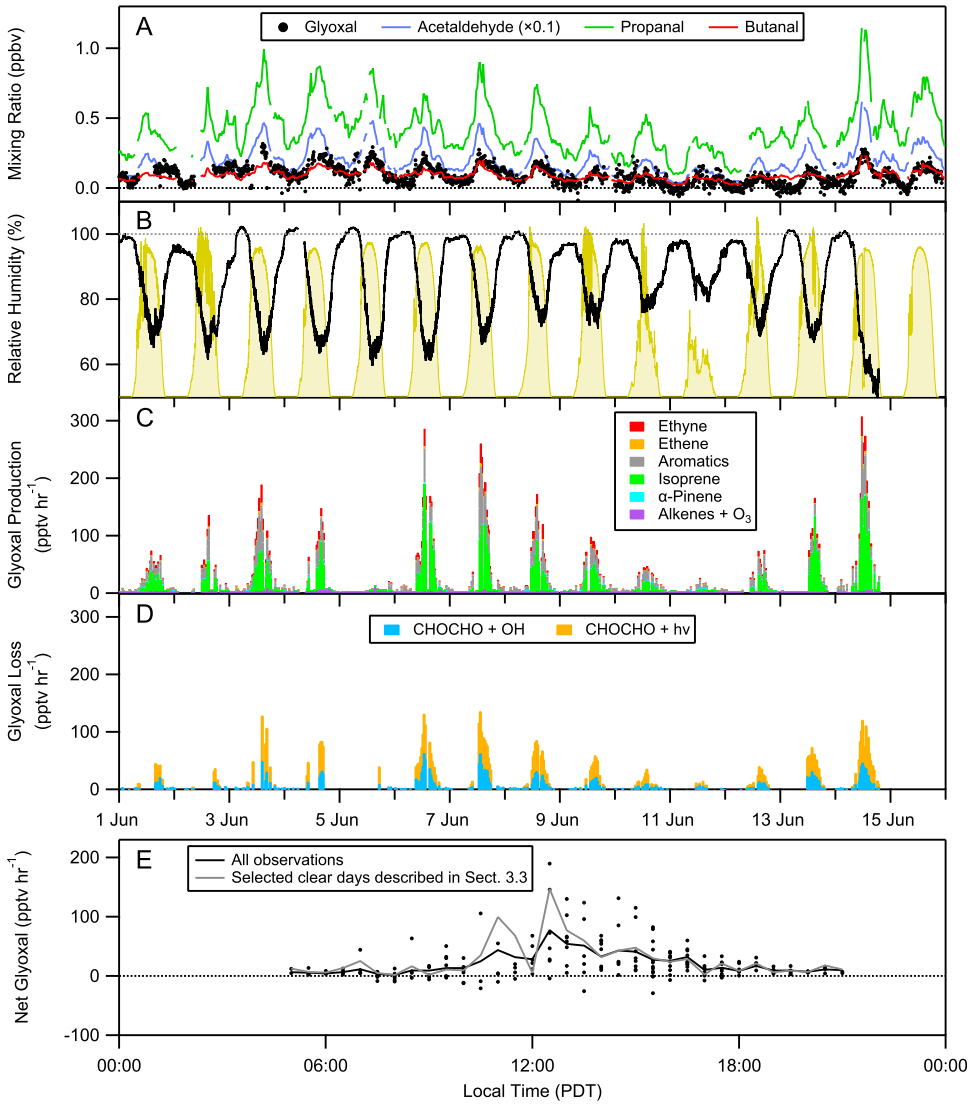

Figure 2. (a) Time series of aldehydes during 1 June to 16 June 2010 showing glyoxal, acetaldehyde, propanal, and butanal. Plotted glyoxal data are 10 min averages. Other aldehydes are measured for 5 min every 30 min. (b) Time series of measured relative humidity and j_{NO2} (yellow bars; units not shown). (c) Time series of the glyoxal production rate calculated from measured VOC, OH, and O_3 concentrations, showing ethyne, ethene, aromatics, isoprene, α-pinene, and alkenes + O_3. (d) Time series of the glyoxal loss rate calculated from CHOCHO + OH and CHOCHO + hν. (e) Net glyoxal calculated from the difference between production (Figure 2c) and loss (Figure 2d), calculated for all observations and for selected dates used in the MCM analysis. Data are shown as a diurnal average.

Hole Oceanographic Institution research vessel (RV) Atlantis, NOAA and CIRPAS Twin Otter aircraft, a second ground site located in Bakersfield, California, and other measurements. Data acquired onboard the NOAA WP-3D aircraft and RV Atlantis are used in this study to quantify trace gas concentrations in the residual boundary layer and Santa Monica Bay. The NOAA WP-3D aircraft acquired VOC samples using a Whole Air Samper (WAS) [*Colman et al.*, 2001]. A chemiluminescence instrument on the NOAA WP-3D measured O_3 [*Ryerson et al.*, 1998], NO [*Ryerson et al.*, 2000], and NO_2 [*Pollack et al.*, 2011]. Onboard the RV Atlantis, a gas chromatograph with flame ionization detection (GC-FID) acquired one 5 min sample every 30 min that included ethyne, ethene, benzene, propane, and n-butane [*Bon et al.*, 2011]. O_3 on the RV Atlantis was measured by UV absorbance, while NO and NO_2 were measured by chemiluminescence [*Williams et al.*, 2009]. Weather conditions at the coast were determined using National Weather Service data from Los Angeles International Airport and GOES 1 km visible satellite images.

3. Results and Discussion

3.1. Glyoxal Mixing Ratios

[18] Figure 2a shows the time series for glyoxal, together with acetaldehyde, propanal, and butanal during 1–16 June 2010. Each of these aldehydes is photochemically produced and lost predominantly through photolysis and reaction with

OH. Figure 2b shows the measured relative humidity and j_{NO2} values during this period. The diurnal cycle for glyoxal follows a similar pattern to the other aldehydes, with an average daytime peak concentration of 160 pptv at 14:30 Pacific Daylight Time (PDT = UTC − 7 h). The relationship between glyoxal and the three aldehydes shown in Figure 2a was fitted using an unweighted linear orthogonal distance regression. The fitted values with 2-σ standard deviations are glyoxal versus acetaldehyde: intercept = 0.001 ± 0.006, slope = 0.050 ± 0.003, and R^2 = 0.60; glyoxal versus propanal: intercept = −0.026 ± 0.008, slope = 0.29 ± 0.02, and R^2 = 0.60; glyoxal versus butanal: intercept = −0.09 ± 0.01, slope = 2.0 ± 0.1, and R^2 = 0.63.

[19] We have used three independent methods to analyze the production and loss budget for glyoxal and the potential for aerosol contribution within this budget: a steady state production and loss budget (section 3.2), a two-dimensional Lagrangian model that employs the Master Chemical Mechanism (section 3.3), and the observed nighttime loss of glyoxal in the absence of its photochemical sources and sinks (section 3.4). The results from these three approaches are discussed in detail below and compared in section 3.5.

3.2. Glyoxal Budget: Steady State Production and Loss

3.2.1. Description of Method

[20] For a species at steady state, the concentration in a fixed volume does not change with time and the sources must be balanced by the sinks. This is a simple method for determining if there is a large discrepancy between the known gas-phase sources and sinks of glyoxal. If the calculated sources exceed the sinks, the discrepancy may be attributed to an additional loss process such as heterogeneous uptake. Using this method requires both assuming that the sources and sinks balance, and that the air basin is homogeneous such that transport may be neglected. This approach is similar to the *Volkamer et al.* [2007] analysis of the glyoxal budget for Mexico City, which quantified the imbalance between sources and sinks for a fixed location neglecting transport.

[21] Figure 2a shows the time series of glyoxal. Glyoxal concentrations were approximately constant (i.e., d[CHOCHO]/dt ≈ 0) during a short period between approximately 13:00–15:00 PDT. The boundary layer height was nearly constant during this period, with the ceilometer measuring an average change from 780 to 880 m (13%). The average lifetime of glyoxal with respect to combined loss by OH and photolysis during 13:00–15:00 PDT is 2.6 h. The steady state approximation requires that a reaction must have proceeded for a period of time several times longer than the lifetime with respect to the loss [*Pilling and Seakins*, 1995]. For the glyoxal budget described here, steady state production and loss may be an inaccurate approximation and should be interpreted cautiously. Section 3.5 describes corrections to this approach based on a model that includes advection.

[22] We calculate the glyoxal sources and sinks at 30-min intervals corresponding to the sampling times for GC-MS measurement of VOCs. Glyoxal is produced as a first-generation oxidation product when OH reacts with ethyne, benzene, toluene, xylene, 1-ethylbenzene, isopropylbenzene, n-propylbenzene, 1,2,3-trimethylbenzene, and 1,2,4-trimethylbenzene. The glyoxal production for these reactions was calculated from published rate coefficients [*Atkinson*, 1994; *Sander et al.*, 2006] and yields [*Fu et al.*, 2008]. Glyoxal is produced as a second-generation oxidation product when OH reacts with ethene, with glycolaldehyde as an intermediate step. We calculated an effective first-order reaction rate for the first 4 h of glyoxal production from ethene using a system of ordinary differential equations, with rate coefficients for ethene + OH [*Atkinson et al.*, 2005] and glycolaldehyde + OH [*Bacher et al.*, 2001], with yields described by *Fu et al.* [2008]. Glyoxal is produced as a first-, second- and third-generation product from isoprene. The first generation glyoxal production from isoprene [*Volkamer et al.*, 2006a; *Galloway*, 2011] was incorporated with a yield of 2.1% [*Galloway*, 2011] and an OH rate coefficient from *Atkinson* [1997]. For the production of glyoxal as a second- and third-generation product from isoprene, we calculated an effective first-order rate coefficient for the first 4 h using a system of ordinary differential equations, with rate coefficients for isoprene + OH [*Atkinson et al.*, 2006], MVK + OH [*Atkinson et al.*, 2006], hydroxymethylvinylketone + OH (from MCMv3.1 [see *Saunders et al.*, 2003]), C_5 unsaturated hydroxy aldehydes + OH [from MCMv3.1; see *Saunders et al.*, 2003], and glycolaldehyde + OH [*Bacher et al.*, 2001], with yields described by *Fu et al.* [2008]. Ozone + alkene reactions typically contribute 1–8% of the daytime glyoxal budget in Pasadena. We include glyoxal yields from ozone reactions with ethene, propene, 1-butene, cis-2-butene, trans-2-butene, 2-methylpropene, 1,3-butadiene, and α-pinene with published yields and rate coefficients [*Calvert et al.*, 2000]. The reaction of ozone with some higher alkenes that were not measured by GC-MS also produces glyoxal [*Calvert et al.*, 2000], but this is expected to be a small part of the total budget. The calculated glyoxal sources are shown in Figure 2c. As described above, isoprene produces glyoxal as a first-, second-, and third-generation product, while ethene produces glyoxal as a first-, and second-generation product. The second- and third-generation production of glyoxal makes an average contribution of 11% to the total glyoxal production rate. Isoprene is the most significant source of glyoxal, accounting for as much as 60% of the production rate during some periods. The laboratory studies for glyoxal yields from isoprene oxidation are recent, and future work may provide revised budgets for isoprene oxidation. The analysis in this section and section 3.3 reflects the current literature for isoprene oxidation.

[23] Two glyoxal sinks were included in the steady state budget: OH reaction and photolysis. Changes due to horizontal advection have been neglected. The rate for glyoxal + OH was calculated from the measured values of each compound, with rate coefficients from *Feierabend et al.* [2008]. Although actinic flux spectra were recorded to calculate photolysis loss rate coefficients (j) for species such as NO_2 and O_3, j_{CHOCHO} has not been reported to date for the Pasadena ground site. Using actinic flux spectra acquired onboard the NOAA WP-3D aircraft, we calculated j_{CHOCHO} [*Feierabend et al.*, 2009], and parameterized its empirical relationship to j_{NO2} and j_{O3} to be $j_{CHOCHO} = j_{NO2} \times (0.010910 \pm 3 \times 10^{-6}) + j_{O3} \times (0.6039 \pm 0.0006)$. This particular parameterization was chosen because the action spectrum (product of absorption and quantum yield) for glyoxal lies spectrally between the action spectra of O_3 and NO_2. The

total error in j_{CHOCHO} from this parameterization is less than ±3% compared to the direct calculation, for solar zenith angle less than 70 deg (~07:30–18:15 PDT). The calculated glyoxal sinks due to OH reaction and photolysis are shown in Figure 2d. Average glyoxal loss by photolysis and OH are 6.2×10^{-5} s^{-1} and 3.8×10^{-5} s^{-1}, respectively, between 12:45–16:00 PDT for the selection of eight clear days described in section 3.3.1, with an average OH value of 4.3×10^6 cm^{-3}. The calculated glyoxal aerosol sink can be compared to these values to determine its relative importance.

3.2.2. Results

[24] The difference between the calculated sources and sinks is shown in Figure 2e. The data are presented both as all data points for a particular time of day and as a diurnal average, which gives an average balance between production and loss not subject to data gaps that occur on any individual day when the multiple data sets are combined. Figure 2e shows that the net yield of glyoxal in the budget is positive. During the period from 13:00–15:00 PDT, the average net production in Figure 2e is 44 ± 9 pptv h^{-1} (error is 1σ). For a selection of eight sunny days (described further in section 3.3.1), the production and loss are both greater, and the average net production is 52 ± 18 pptv h^{-1}. If the glyoxal budget were at steady state, then the sources and sinks would be equal, and any discrepancy could be directly attributed to an additional glyoxal loss, which prior laboratory and field studies would suggest is due to a heterogeneous loss process (equivalent to 0.10 and 0.12 μg m^{-3} h^{-1} for 44 pptv h^{-1} and 52 pptv h^{-1} respectively). A correction to the steady state approximation, based on the two-dimensional pseudo-Lagrangian model, is presented in section 3.5.

3.3. Glyoxal Budget: Master Chemical Mechanism

3.3.1. Description of Method

[25] We modeled gas-phase production and loss of glyoxal using a two-dimensional pseudo-Lagrangian model, and compared the results to the measured glyoxal concentrations in Pasadena. Because the model does not include heterogeneous loss processes, the difference between the modeled and measured glyoxal concentrations can be used to constrain the magnitude of such loss mechanisms. The model used in this work is a subset of the MCM version 3.2, a near-explicit representation of the degradation of VOCs [*Jenkin et al.*, 2003; *Saunders et al.*, 2003; *Bloss et al.*, 2005]. It incorporates measured kinetic and product data when available, along with structure-activity relationships for unmeasured reactions, to model the formation of secondary photochemical products. The subset described here includes a complete inorganic mechanism and the oxidation mechanisms for 62 VOCs, including all of the species described in section 3.2. The mechanism for the 62 VOCs included 3677 species and 11157 reactions. We modified the MCM to include the first generation production of glyoxal and glyocoaldehyde from isoprene + OH, with yields of 2.1% [*Volkamer et al.*, 2007; *Galloway*, 2011] and 2.7% [*Galloway*, 2011], respectively. These two sources were an addition to the standard MCM v3.2 mechanism for isoprene oxidation, which we did not change and which includes glyoxal formation from glycolaldehyde.

[26] We use the MCM model to simulate the chemical composition of an air parcel as it is advected across the Los Angeles basin. This approach is pseudo-Lagrangian, because it uses dilution to account for changes in the boundary layer height. We selected model days with simple, direct transport from the coast to Pasadena under sunny, cloud-free, and fog-free conditions. These conditions led to repeatable sea breeze meteorology and advection, as confirmed using back trajectory analysis. During partly cloudy or foggy days, advection patterns can be more complicated, and it is difficult to accurately represent glyoxal photolysis rates and OH concentrations. We have not analyzed glyoxal processing in clouds for this study.

[27] The average wind speed and direction during the field campaign is shown in wind rose plots in Figure 1b. Selection of days was based on three pieces of meteorological data: 1) clear conditions between 13:00–17:00 PDT in Pasadena indicated by j_{NO2}; 2) cloud-free conditions at 13:00 PDT in GOES 1 km visible satellite images along the Santa Monica Bay coast near Los Angeles International Airport; and 3) back trajectories that indicated direct transport from the coast inland to Pasadena. Based on these three criteria, eight of the 18 days were selected: 30 and 31 May 2010, and 3, 4, 5, 7, 14, and 15 June 2010. The discussion of the MCM model results refers to the average of these eight selected days.

[28] For the selected days, the average transport time and boundary layer evolution was determined from the Advanced Research Weather Research and Forecasting (WRF) model version 3.2.1 with 12 × 12 km horizontal grid and 40 vertical levels [*Skamarock et al.*, 2008]. Key physics options were the 5-layer thermal diffusion land surface, Mellor-Yamada-Janjic (MYJ) PBL scheme, and Rapid Radiative Transfer Model (RRTMG) long- and shortwave radiation. Wind speed and direction were averaged between the surface and 500 m for the back-trajectory calculations of transport time in the planetary boundary layer. For the eight selected days, an average transport time of 3.25 h between the coast and Pasadena was calculated for air parcels arriving at 16:00 PDT. Figure 1 shows the average WRF back trajectory, with tick marks indicating 30 min of transport time. The observed local surface wind speeds and directions shown in Figure 1b are consistent with the calculated WRF back trajectories. In the analysis that follows, we have made the simplified assumption that transport speed is constant between the coast and Pasadena.

[29] The boundary layer height was modeled using WRF for each of the eight days. The modeled time period of 12:45–16:00 PDT is mid to late afternoon, and WRF modeling indicated that the boundary layer was well-developed. Based on the WRF model results, we employed a boundary layer of 400 m at the coast growing linearly to 800 m above ground level (AGL) at the Pasadena field site. This is consistent with the average ceilometer height of 740 m at 16:00 PDT for the selected days. This was represented as a dilution term in the MCM model. Model starting concentrations for ethyne, ethene, toluene, benzene, propane, n-butane, O_3, and NO_x were determined from RV Atlantis measurements in Santa Monica Bay between 13:00–14:00 PDT on 24 May 2010 and 30 May 2010, which are the periods when the ship was in this region, representing the coastal air mass upwind from Pasadena at the beginning of the 3.25 h transport time. Model starting conditions for VOC precursors that were not measured by the GC-FID instrument onboard the RV Atlantis were determined from measurements by the WP-3D aircraft at altitudes less than 350 m during vertical profiles

Table 2. Master Chemical Mechanism Model Results and Comparison to Measurements

VOC	Initial Concentration (ppbv)	Residual BL Concentration[a] (ppbv)	Emission Ratio VOC/C_2H_2	Measured Concentration[b] (ppbv)	Modeled Concentration[c] (ppbv)	Model-Measured Difference[d] (%)
Ethyne	0.12[e]	0.24	1.00[f]	1.78	1.78	0
Ethene	0.065[e]	0.065	1.36[f]	2.16	1.88	−13
Benzene	0.039[e]	0.040	0.19[f]	0.36	0.34	−4
Toluene	0.017[e]	0.028	0.82[f]	0.83	1.19	44
m,p-Xylene	0[g]	0	0.37[f]	0.32	0.40	26
o-Xylene	0[g]	0	0.14[f]	0.14	0.17	21
1-Ethylbenzene	0[g]	0.003	0.10[f]	0.14	0.14	2
n-Propylbenzene	0[g]	0	0.028[f]	0.022	0.040	82
Isopropylbenzene	0[g]	0	0.009[f]	0.007	0.013	86
1,2,3-Trimethylbenzene	0[g]	0	0.027[f]	0.029	0.022	−24
1,2,4-Trimethylbenzene	0[g]	0	0.12[f]	0.089	0.10	16
Isoprene	0[g]	0.003	N/A	1.09	1.09	0
alpha-Pinene	0[g]	0	N/A	0.052	0.052	0
Methyl vinyl ketone	0.14[g]	0.065	1.6×10^{-3}[h]	0.48	0.41	−14
Methacrolein	0.006[g]	0.008	4.8×10^{-3}[h]	0.18	0.24	37
Glyoxal	0	0	6.5×10^{-5}[h]	0.19	0.18	−5
Acetaldehyde	0.26[i]	0.5[j]	0.5[f]	3.39	2.19	−35

[a]From Whole Air Sample measurements onboard the NOAA WP-3D aircraft acquired during three profiles above Los Angeles International Airport between 13:30–17:30 PDT on 8 May and 20 June 2010. Zero indicates measurements below the detection limit.
[b]Average concentration observed at Pasadena ground site for 16:00 PDT during eight clear days between 30 May to 15 June 2010.
[c]MCM v3.2 model prediction for 16:00 PDT.
[d]100 × (Modeled Concentration – Measured Concentration)/Measured Concentration.
[e]From GC-FID measurements onboard the RV Atlantis within the Santa Monica Bay between 13:00–14:00 PDT on 24 May 2010 and 30 May 2010.
[f]From *Warneke et al.* [2007]. Average of Boston/New York City values reported for 2002 and 2004.
[g]From Whole Air Sample measurements onboard the NOAA WP-3D aircraft acquired below 350 m near Catalina Island, 47 km south of Santa Monica Bay, between 11:30–13:30 PDT on 4 May, 16 May, and 20 June 2010. Zero indicates measurements below the detection limit.
[h]From *Ban-Weiss et al.* [2008] aldehyde/CO ratios multiplied by CO/C_2H_2 (Pollack et al., manuscript in preparation, 2011).
[i]From PTR-MS measurements onboard the NOAA WP-3D aircraft acquired below 350 m near Catalina Island, 47 km south of Santa Monica Bay, between 11:30–13:30 PDT on 4 May, 8 May, 16 May, and 20 June 2010.
[j]From PTR-MS measurements onboard the NOAA WP-3D aircraft acquired during three profiles above Los Angeles International Airport between 13:30–17:30 PDT on 8 May and 20 June 2010.

near Catalina Island (47 km south of Santa Monica Bay) between 11:30–13:30 PDT on 4 May, 8 May, 16 May, and 20 June 2010. Initial concentrations are shown in Table 2.

[30] VOC, O_3, and NO_x concentrations in the residual boundary layer were determined from three WP-3D vertical profiles at Los Angeles International Airport conducted between 13:30–17:30 PDT on 8 May and 20 June 2010. The residual boundary layer measurements are shown in Table 2. As described above, the boundary layer growth between the coast and the Pasadena field site was represented as a dilution term in the model. Instead of adding a dilution of clean air, VOC concentrations from the polluted residual boundary layer were added at a rate equal to the dilution term.

[31] Because Los Angeles is a densely populated urban area, we assumed that anthropogenic emissions were constant along the 3.25 h trajectory from the coast to Pasadena, with a constant ethyne emission rate optimized to match the Pasadena measurements. Comparison to the 2005 National Emission Inventory showed that this emission rate was reasonable. Reported values by *Warneke et al.* [2007] were used to constrain the emission ratios of anthropogenic alkanes, alkenes, aromatics, acetaldehyde, propanal, and methylethylketone relative to ethyne. Other aldehyde emission ratios were taken from measurements acquired in a San Francisco area highway tunnel bore during 2006 [*Ban-Weiss et al.*, 2008], weighted by relative gasoline and diesel fuel sales in California during June 2010 reported by the California State Board of Equalization. California gasoline formulations have specifically addressed the reduction of aldehyde emissions, and direct emissions by vehicles represent a small fraction of the total budget for glyoxal and other aldehydes. Ethanol is an acetaldehyde precursor whose emissions have increased due to changing fuel composition in the U.S. [*Naik et al.*, 2010]. For this reason, we empirically adjusted the ethanol/ethyne emission ratio to match the observations in Pasadena, rather than using literature values. NO emission was also assumed to be constant relative to ethyne, with a NO_x/C_2H_2 emission ratio of 27.1 for weekdays and 19.5 for weekends, which was calculated from I. B. Pollack (Airborne observations of the weekend ozone effect and precursor emissions in the California South Coast Air Basin during CalNex, submitted to *Journal of Geophysical Research*, 2011). Table 2 gives a selected set of VOC emission ratios for glyoxal precursors.

[32] As discussed above, biogenic VOCs are important glyoxal precursors. The ratio of isoprene to its first generation oxidation products, MVK and methacrolein, was large (1.7), suggesting recent biogenic VOC emissions in air at the Pasadena site. To best reproduce these observations, the emissions for isoprene and α-pinene were each set to constant rates for the first 2.4 h (~28 km) of the transit, and then to higher constant rates for the final 0.8 h (~9 km) transit. The time division was selected to approximately match the vegetation coverage observed in visible satellite images. In addition, isoprene emissions vary diurnally with meteorological conditions, and higher emission rates are expected during the late afternoon [*Guenther et al.*, 1993]. The isoprene emission rates for the two sections of transport were

adjusted empirically to optimize the agreement between observed and modeled isoprene, the sum of MVK and methacrolein, and the ratio of isoprene to the sum of MVK and methacrolein. The α-pinene emission rates were adjusted empirically to match the observed value, with the ratio between the α-pinene emission rates for the first 2.4 h and final 0.8 h of transit constrained to the ratio of the isoprene emission rates.

[33] Photolysis rate constants, OH, and O_3 in the model were constrained to measured values. The average diurnal OH measurements at Pasadena were assumed to be representative across the air mass trajectory. O_3 was constrained by the measurements in Santa Monica Bay (52.3 ppbv) and in Pasadena (70.5 ppbv), with a linear increase. The photolysis rate constants as a function of time-of-day are calculated using the MCM parameterization for the latitude and longitude of the field study, scaled to the j_{NO2} value measured in Pasadena.

[34] To independently examine the predictive accuracy of the model, we have included the precursors and chemistry for acetaldehyde, which is not believed to have heterogeneous loss processes. Acetaldehyde was selected as an analog for glyoxal because 1) it has photochemical sources and sinks; 2) it has fewer sources and lower background concentrations than formaldehyde; and 3) accurate measurements are available for the Pasadena field site. The major acetaldehyde precursors are ethane, propane, isopentane, 3-methyl-pentane, 2-methyl-pentane, n-butane, propene, 1-butene, isoprene, and ethanol [*Lewis et al.*, 2005; *Millet et al.*, 2010]. The model starting conditions and residual boundary layer concentrations for acetaldehyde and its precursors were determined using RV Atlantis and WP-3D measurements as described above.

3.3.2. Results

[35] For the model inputs described above, the MCM model predictions for VOC concentrations at 16:00 PDT in Pasadena are shown in Table 2, together with the average measured values and percent difference. The difference between the measured and modeled precursor concentrations does not follow a trend with OH reactivity, and hence does not suggest an error in transport time or OH concentration. The greatest discrepancies between measured and modeled precursor concentrations are observed for n-propylbenzene and isopropylbenzene, which are present at the lowest concentrations and have the most uncertain emission ratios. The evolution of anthropogenic precursors, biogenic precursors, and glyoxal are shown in Figure 3 as a function of time and transport distance.

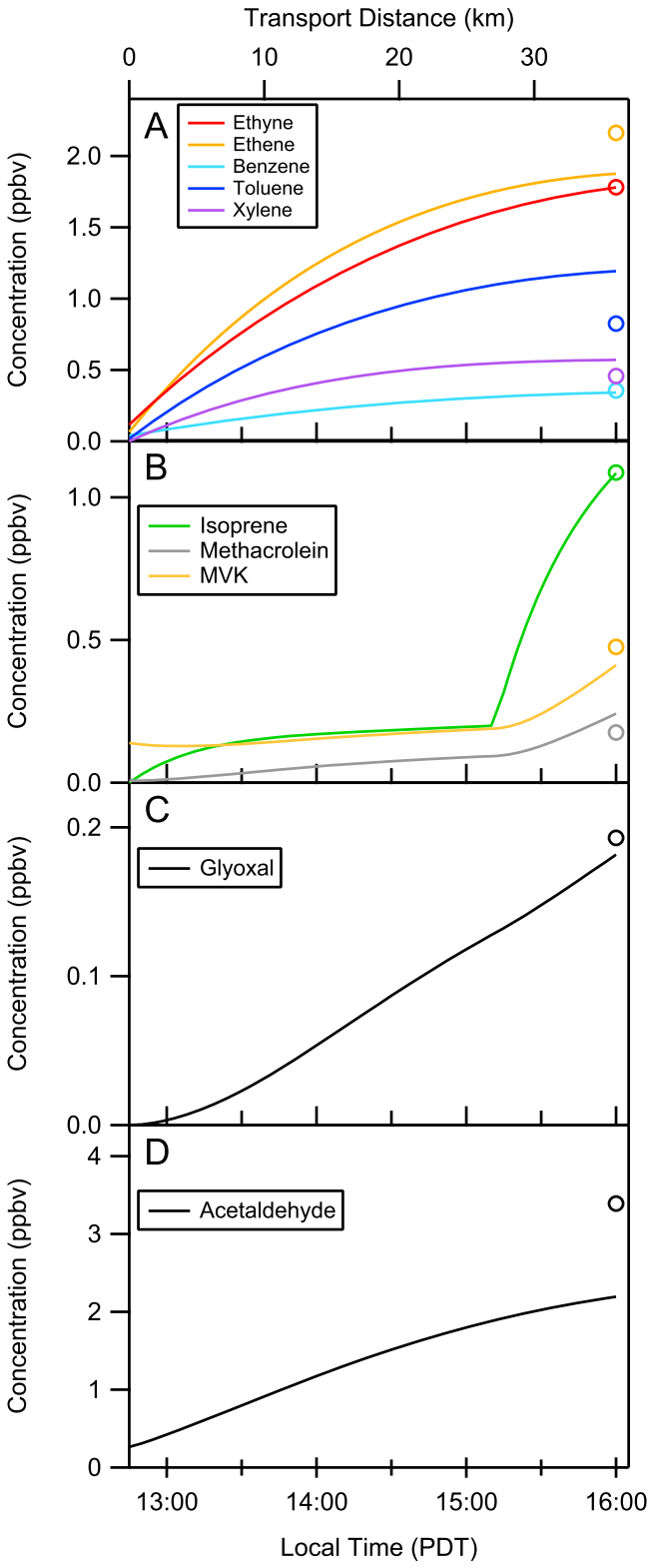

Figure 3. Results from the Master Chemical Mechanism v3.2 "base case" model. These results are presented numerically in Table 2. VOC concentrations are plotted for an air parcel that starts at the coast (time = 12:45 PDT; distance = 0 km) and arrives at the CalNex ground site (time = 16:00 PDT; distance = 37 km). (a) Modeled anthropogenic concentrations for ethyne, ethene, benzene, toluene, and xylenes as a function of transport time. Average values measured at the CalNex ground site at 16:00 PDT are shown as open circles. (b) Modeled biogenic concentrations for isoprene and its oxidation products methacrolein and MVK. Average values measured at the CalNex ground site at 16:00 PDT are shown as open circles. (c) Modeled glyoxal concentrations as a function of transport time. Average value measured at the CalNex ground site at 16:00 PDT is shown as an open circle. (d) Modeled acetaldehyde concentrations as a function of transport time. Average value measured at the CalNex ground site at 16:00 PDT is shown as an open circle.

[36] As shown in Figure 3 and Table 2, the MCM model reproduces the measured glyoxal concentration to within 5%. Although the model underpredicts the measurement, this error is within the combined uncertainties of the measurement (±15%) and model, and therefore represents essentially quantitative agreement. However, the model also underpredicts the measured acetaldehyde by a larger factor (35%). Since glyoxal has a smaller number of sources than acetaldehyde, we expect that its chemistry is better constrained by the model. However, the underprediction of acetaldehyde in the model may indicate a more general underprediction in the production of aldehydes across the Los Angeles basin. If so, then the model predictions of glyoxal may also be too low. Therefore, assuming that the difference between the modeled and measured glyoxal concentrations can be attributed to heterogeneous uptake, we constrain the fraction of glyoxal that contributes to heterogeneous loss to be 0–30%, where the low end of the range is the direct model prediction and the upper end of the range is corrected by the underprediction of acetaldehyde (i.e., −5 + 35%). A glyoxal sink of 0–30% after 3.25 h corresponds to a loss rate coefficient with respect to heterogeneous loss of $0–5 \times 10^{-5}$ s^{-1}.

[37] We varied the model input parameters through a series of sensitivity tests. The choice to constrain the emission ratios of all VOCs to published values [*Warneke et al.*, 2007; *Ban-Weiss et al.*, 2008] was made to realistically constrain the model to established measurements of anthropogenic emissions. However, Table 2 shows that this constraint results in modeled VOC concentrations that do not match measurements in all cases. To explore this discrepancy, we performed additional model runs with the emission ratio constraints removed. We empirically adjusted the emission rate of ethene and the aromatic glyoxal precursors to a constant rate to best match the observed concentrations in Pasadena. In the model, each VOC was emitted at a constant rate during the transport time, but the ratios of the rates were not constrained. Optimizing the VOC emission rates independently reduces the modeled glyoxal concentration from 181 pptv to 154 pptv, increasing the discrepancy with the measurements.

[38] As a second sensitivity test, we replaced the constant anthropogenic emission rates with different spatial distributions of emissions. Although the entire Los Angeles Basin is densely populated, anthropogenic emission rates are likely to be greatest near downtown Los Angeles (corresponding approximately to the middle 1.6 h of transport) and lower in the vicinity of Pasadena (corresponding approximately to the final 0.8 h of transport, where biogenic emissions are greatest). In the first spatial emissions test, we set the emission rate to a constant during the first 2.4 h of transport, and then reduced the emission rate by a factor of two during the final 0.8 h of transport. The anthropogenic emission ratios were constrained to ethyne, and we adjusted the ethyne emission rates to match to its measured concentration. The discrepancy between modeled and measured glyoxal and acetaldehyde were 1.6% and −32.9%, respectively. In the second spatial emission test, we set the emission rate to a constant during the first 0.8 h of transport, then increased the emission rate by a factor of two during the middle 1.6 h of transport, and set it to the lower initial value for the final 0.8 h. The discrepancy between modeled and measured glyoxal and acetaldehyde were −4.7% and −34.9%, respectively. These large changes in the spatial distribution of the anthropogenic emissions resulted in relatively small differences in the modeled glyoxal and acetaldehyde concentrations.

[39] As a third sensitivity test, we varied the transport time from the coast to Pasadena in 30 min increments from 2.25 to 4.25 h. The boundary layer was still assumed to begin at 400 m and increase linearly to 800 m between the coast and Pasadena, with mixing in of a polluted residual boundary layer. The emission of ethyne was adjusted to match the measurements in Pasadena. The other VOC emissions were again constrained by their emission ratios to ethyne. Isoprene was still represented as two constant emission rates, one during the first 28 km of transport and a higher rate during the final 9 km. The two emission rates were iteratively adjusted to match the observed isoprene, the sum of MVK and methacrolein, and the ratio of isoprene to the sum of MVK and methacrolein. The results showed the discrepancy between modeled and measured glyoxal concentrations varied from −28% to 10% from shortest to longest transport time, while acetaldehyde error was −40% to −31%. The modeled glyoxal, scaled to acetaldehyde, produced at most an excess of 41% (i.e., 10 + 31%).

[40] As a fourth sensitivity test, we increased the glyoxal concentrations in the starting condition and residual boundary layer. Based on the correlation between glyoxal and acetaldehyde observed in Pasadena during the CalNex field campaign (slope = 0.050), we tested glyoxal starting condition and residual boundary layer values equivalent to 5% of the measured acetaldehyde values (13 and 30 pptv, respectively) and 10% of the measured acetaldehyde values (26 and 59 pptv, respectively). These two scenarios increased the modeled glyoxal, and resulted in a difference between modeled and measured glyoxal of 0% and +6%.

[41] Additional tests were performed to determine the model sensitivity to changes in photolysis, OH, and boundary layer height. To test the model sensitivity to photolysis, we scaled the photolysis rate constants by ±20% in two separate cases, and then adjusted the emissions of ethyne, isoprene, and α-pinene to match the observations as described previously, with the other anthropogenic precursors constrained to the emission rate of ethyne. We expect that this range of values brackets the possible variation in photolysis rate constants along the transport trajectory, because the selected days were cloud-free and photolysis rates were scaled by the measured j_{NO2} in Pasadena. The resulting differences between modeled and measured glyoxal were −10% and 0%, due to changes in j_{CHOCHO}, when photolysis rates were increased and decreased by 20%, respectively. The change in modeled acetaldehyde was less than 1%. To test the model sensitivity to OH, we scaled its measured concentration by ±50% in two separate cases, and again adjusted the emissions of ethyne, isoprene, and α-pinene to match the observations. This large variation was chosen because the model was constrained by OH concentrations at the CalNex ground site, which may be lower than the upwind portion of the trajectory due to the higher local concentrations of isoprene at the Pasadena field site. The resulting differences between modeled and measured glyoxal were −45% and 25%, while acetaldehyde differences were −43% and −30%, respectively for decreased and increased OH. Finally, we varied the gradient in boundary layer height, with a

400 m boundary layer at the coast and a 600 or 1000 m boundary layer in Pasadena, with the dilution rate, ethyne, isoprene, and α-pinene emissions adjusted accordingly. The modeled glyoxal showed only a weak dependence on the boundary layer profile, with differences between model and measurement of −4% to −7%, respectively for the 600 and 1000 m cases. In summary, changes in emission ratios, transport time, starting and boundary layer conditions, photolysis rates, and boundary layer height each have a small influence on the model results for realistic ranges of the possible input parameters, while OH changes the results more significantly, in part because of the large selected range in the sensitivity test.

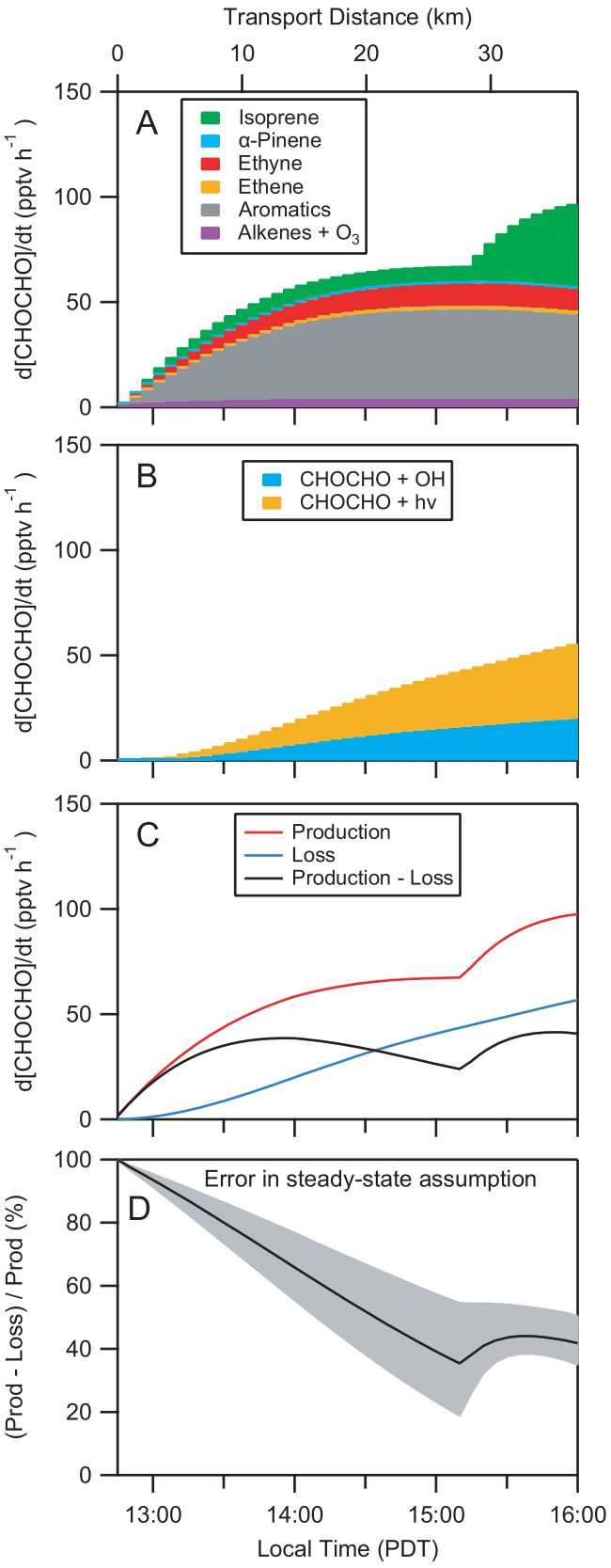

Figure 4. Instantaneous production and loss of glyoxal, calculated for each step of the MCM v3.2 "base case" model. (a) Glyoxal production from ethyne, ethene, isoprene, α-pinene, aromatics, and alkenes + O_3. (b) Glyoxal loss by photolysis and OH. (c) Instantaneous production, loss, and net production calculated from the difference. (d) Net production as a fraction of the total production (black line), indicating the deviation from steady state. Shaded gray area shows the results when the OH concentration in the model is scaled by ±50%.

[42] As a final examination of the MCM model output, Figure 4 shows instantaneous production and loss rates for glyoxal during each 5-min time step. Production and loss are calculated identically to that described in section 3.2 for the steady state budget, except using the VOC, OH, and photolysis rates from the model at each step. The difference between production and loss relative to the total production, i.e., (P − L)/P, as shown in Figure 4c, indicates that glyoxal approaches steady state over the course of the trajectory, but has not reached steady state as the air mass arrives at the CalNex field site at 16:00 PDT. The modeled difference between production and loss is 42% of the total production at that time, and is due solely to the accumulation of glyoxal in the gas phase.

3.4. Glyoxal Budget: Nighttime Loss

3.4.1. Description of Method

[43] The third approach for quantifying the heterogeneous uptake of glyoxal was to examine nighttime loss rates. Chamber and laboratory studies have observed glyoxal uptake to inorganic aerosol seed that occurs in the absence of light [*Kroll et al.*, 2005; *Liggio et al.*, 2005a; *Corrigan et al.*, 2008; *Galloway et al.*, 2009; *Volkamer et al.*, 2009]. Glyoxal is a secondary photochemical product, with minor direct emissions [*Ban-Weiss et al.*, 2008]. In the gas-phase, it is lost by reaction with OH and photolysis. Higher aldehydes (e.g., acetaldehyde, propanal, and butanal) have similarly minor direct emissions, and their gas-phase production and loss are each dominated by photochemical processes. If there are significant heterogeneous loss processes that occur in the absence of light, these should be measurable at night. The change in glyoxal concentration at night can be compared directly to higher aldehydes (acetaldehyde, propanal, and butanal) measured in Pasadena. The butanal uptake by inorganic aerosol has been observed to be 7–28 times less than that for glyoxal [*Jang and Kamens*, 2001]. Acetaldehyde and propanal uptake by SOA is expected to be even less than that of butanal [*Jang and Kamens*, 2001].

3.4.2. Results

[44] Figure 5 shows the diurnally averaged acetaldehyde, propanal, butanal, and glyoxal concentrations averaged for

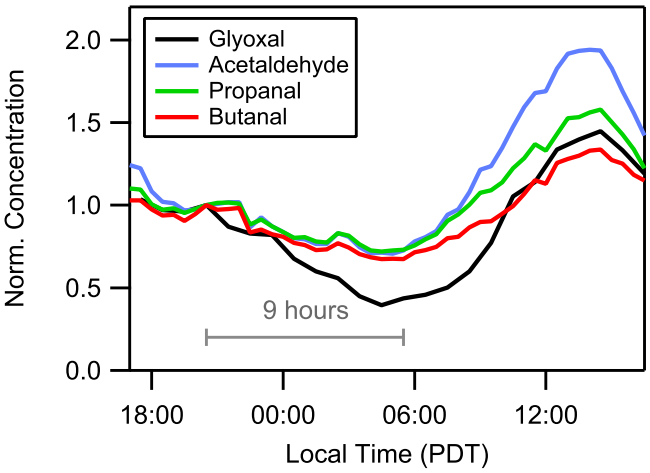

Figure 5. Diurnally averaged glyoxal, acetaldehyde, propanal, and butanal. Each trace is normalized to 1.00 at 20:30 PDT. The change in acetaldehyde, propanal, and butanal during the 9 h period from 20:30–05:30 PDT is −30% ± 6%, while the corresponding change in glyoxal is −56%.

29 May to 16 June 2010. For each species, the concentration has been normalized to that at 20:30 PDT, so that the relative loss rates can be directly compared. Unlike the daytime modeling presented in section 3.3, the nighttime loss rates are presented for all days, without selection for specific daytime meteorology. The measured Henry's Law constants at 298 K in pure water for glyoxal, acetaldehyde, propanal, and butanal are 4.19×10^5 [*Ip et al.*, 2009], 14.9, 12.2, and 8.7 M atm^{-1} [*Zhou and Mopper*, 1990], respectively. Relative humidity was typically high during the night, with diurnally averaged values increasing from 82% at 20:30 PDT to 97% at 5:30 PDT. Over the nine hour nighttime period from 20:30–5:30 PDT, there is a clear difference between glyoxal and the three higher aldehydes. The average concentration change for the three higher aldehydes over the nine hour period is −30 ± 6% (where 6% is the range of values for the three aldehydes), while glyoxal shows a concentration change of −56% during the same period. Aldehyde loss by reaction with OH and O_3 are both negligible, due to the low nighttime concentrations of OH (approximately 2×10^5 cm^{-3}) and the extremely slow reaction of O_3 with glyoxal and other aldehydes [*Atkinson et al.*, 1981; *Plum et al.*, 1983]. The average NO_3 concentrations observed in the lowest DOAS slant path during this 9 h period is 7.4 pptv. For a maximum NO_3 concentration of 10 pptv persisting through the night and literature reaction rate constants [*Atkinson et al.*, 2005], this would remove 2.1%, 5.2%, and 8.9% of acetaldehyde, propanal, and butanal, respectively. The glyoxal rate constant with NO_3 has not been reported. Nighttime production of glyoxal by ozone + alkene reactions contributes less than 3 pptv h^{-1} and is neglected here.

[45] If the loss of glyoxal relative to the other aldehydes is attributed to heterogeneous aerosol uptake processes, the observed nighttime loss can be used directly to calculate a first-order loss rate constant. If we assume that the 30% loss observed for acetaldehyde, propanal, and butanal can be attributed to a loss process shared with glyoxal that does not contribute to SOA mass, such as a combination of transport, dilution by cleaner air (e.g., downslope flow from the nearby foothills), and reaction with NO_3, then 26 ± 6% of the initial glyoxal concentration is lost over 9 h to aerosol. Calculating the first-order loss rate coefficient as ln(1 − 0.26)/9 h, gives $(1 \pm 0.3) \times 10^{-5}$ s^{-1}.

3.5. Glyoxal Contribution to SOA: Comparison of the Three Methods

[46] Laboratory studies indicate that aqueous-phase photochemistry enhances glyoxal uptake during the day, and also that glyoxal uptake depends on liquid water content. The first two methods address the daytime contribution of glyoxal to SOA. The first method is a steady state budget, applied during 13:00–15:00 PDT. We have assumed a steady state glyoxal concentration and attributed the difference between production and loss to an aerosol loss process. With this assumption, we find that the magnitude of this loss process would be 44 ± 9 pptv h^{-1} for all days and 52 ± 18 pptv h^{-1} for a selection of eight clear days. The lifetime of glyoxal with respect to OH and photolysis is 2.6 h during the afternoon time period, indicating that glyoxal is unlikely to have reached steady state. Further evidence from the calculation of instantaneous production and loss for the MCM model time steps, shown in Figure 4, shows that production exceeds loss and confirms that glyoxal is not at steady state as it arrives in Pasadena. Figure 4d indicates that the difference from steady state is large early in the trajectory, and remains at 42% when the air mass arrives in Pasadena at 16:00 PDT. Applying this as a correction to the steady state analysis for the selection of clear days, we find that −5 ± 18 pptv h^{-1} can be attributed to deposition. For all of the days, the corrected value is 0 ± 9 pptv h^{-1}, although the 42% correction is only strictly appropriate for sunny days. This corrected glyoxal loss rate corresponds to first order heterogeneous loss rates of 0 with an uncertainty of 2×10^{-5} s^{-1}, for both cloudy and clear days.

[47] The second method is a pseudo-Lagrangian model that includes emissions of glyoxal and acetaldehyde precursors. The second method shows that at 16:00 PDT, there is a 0–30% discrepancy between the measured and modeled glyoxal concentration that could be attributed to an aerosol loss process, equivalent to a heterogeneous loss rate coefficient of 0–5 × 10^{-5} s^{-1}.

[48] The third method quantifies the potential nighttime contribution of glyoxal to SOA. This method shows that glyoxal undergoes greater loss than the other aldehydes, with a calculated first-order loss rate coefficient of $(1.0 \pm 0.3) \times 10^{-5}$ s^{-1}. This may be due to the greater Henry's Law constant of glyoxal compared to other aldehydes.

[49] Heterogeneous loss of glyoxal can be attributed to both wet (i.e., aerosol) and dry (i.e., ground or other surface) deposition. For a given species, the rate of dry deposition depends on the height of the boundary layer, surface composition, surface roughness, humidity, and other factors. The dry deposition velocity of acetaldehyde has been measured to be 0.26 ± 0.03 cm s^{-1} for a tropical rain forest [*Karl et al.*, 2004] and 0.2 cm s^{-1} for an alfalfa field [*Warneke et al.*, 2002]. Recently, *Huisman et al.* [2011] reported that the overnight decrease in glyoxal concentrations observed at a rural, forested site could be fit with an exponential loss rate of $(-2.1 \pm 0.3) \times 10^{-5}$ s^{-1}. The measurements and analysis of Huisman et al. are similar to the approach presented in

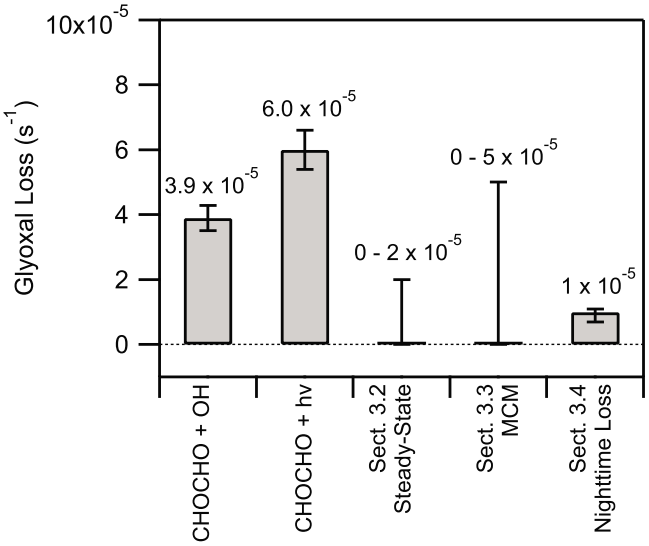

Figure 6. Bar plot showing glyoxal loss to photolysis and reaction with OH, compared to its loss to aerosol formation determined using three methods.

section 3.4, but were conducted under dry conditions (~46% RH) with low available aerosol surface area (~100–200 mm^2 m^{-3}), and not corrected relative to other aldehyde loss rates. This allowed the authors to directly attribute the loss to dry deposition, with a calculated dry deposition velocity of 0.15 cm s^{-1}. This is a lower limit, because other production and loss processes for glyoxal at night are neglected.

[50] If we assume that the dry deposition rate coefficient for glyoxal at the Pasadena field site falls into the range 0.15–0.25 cm s^{-1}, we can calculate how this affects the three heterogeneous loss rates given above. For a daytime boundary layer height of 800 m, the calculated dry deposition loss is 2–3 × 10^{-6} s^{-1}. For the daytime glyoxal loss, the calculated contribution of dry deposition (2–3 × 10^{-6} s^{-1}) is small relative to the total uncertainty in the glyoxal loss rate (0 ± 2 × 10^{-5} and 0–5 × 10^{-5} s^{-1} from the two daytime methods), and we have not explicitly applied the correction. Recent work indicates that deposition rates in vegetated areas may be larger during the day than inferred from nighttime data [*Karl et al.*, 2010], and this could ultimately increase the relative importance of dry deposition to the daytime loss. For the nighttime glyoxal loss, we note that despite its large Henry's Law constant, the reported dry deposition velocity for glyoxal is similar to acetaldehyde. This implies that a correction is not necessary for the nighttime budget of glyoxal, which was already corrected by comparison to acetaldehyde, propanal, and butanal, and that the glyoxal loss can be attributed to aerosol uptake (i.e., wet deposition). However, if the deposition velocity of glyoxal were larger than that of the other aldehydes, then some fraction of the nighttime loss would be due to dry deposition.

[51] The results from the three methods are plotted in Figure 6, as first-order loss rates, and are compared to the average glyoxal loss by OH and photolysis during 12:45–16:00 PDT on the eight selected days. We find that glyoxal contribution to SOA may be of the same order as its OH and photolysis loss rate. Within the error bars, there is no significant difference between the daytime and nighttime loss rates. The three analysis methods do not give any evidence regarding the reversibility of glyoxal uptake to aerosol.

[52] Between 07:00–15:00 PDT, measurements by the AMS at the Pasadena field site show that the diurnally averaged organic aerosol mass increases from 4.8 μg m^{-3} to a maximum of 12.1 μg m^{-3},while the secondary organic aerosol mass (reported as oxygenated organic aerosol) increases from 3.2 μg m^{-3} to a maximum of 8.8 μg m^{-3}. The range of daytime heterogeneous loss rate constants for the two methods reported above is 0–5 × 10^{-5} s^{-1}, corresponding to 0–30% of glyoxal available for uptake by aerosol. Including both the 0–30% of glyoxal available for uptake and the ±15% absolute uncertainty in the glyoxal measurement, we constrain the photochemical glyoxal contribution to secondary organic aerosol mass to be 0–0.2 μg m^{-3} or 0–4%.

[53] The first-order loss rates can be used directly to estimate an aerosol uptake coefficient, γ, which includes all of the processes that affect the rate of gas uptake, including the mass accommodation coefficient at the surface. For small values of γ (i.e., $\gamma < 0.1$) and for uptake to smaller diameter particles (i.e., accumulation mode, <1 μm), the aerosol uptake coefficient can be expressed as

$$k = \frac{1}{4}\bar{c}\gamma S \quad (1)$$

where k is the first-order rate constant, c is the mean molecular speed for glyoxal (324 m s^{-1} at 288 K), and S is the surface area [*Fuchs and Sutugin*, 1971]. The average aerosol dry surface area (7–690 nm) in Pasadena calculated from the SMPS for 12:45–16:00 during the eight clear days and 20:30–05:30 PDT for all days are 498 ± 101 μm^2 cm^{-3} and 213 ± 91 μm^2 cm^{-3}, respectively. After applying the relative humidity scaling (1 + 5.9672 × 10^{-6} RH$^{2.0868}$ + 3.4005 × 10^{-5} RH$^{2.1255}$)^2) reported by *Brown et al.* [2009] to account for the hygroscopic diameter growth between the dry measured and wet ambient particles, the average aerosol surface area is 796 ± 200 μm^2 cm^{-3} and 550 ± 260 μm^2 cm^{-3}, respectively. This gives aerosol uptake coefficients of 0–8 × 10^{-4} and 2 × 10^{-4} ± 1 × 10^{-4} for the day and night, respectively.

[54] In Mexico City, a glyoxal aerosol sink of 2.7–4.2 × 10^{-4} s^{-1} was observed [*Volkamer et al.*, 2007]. This is one to two orders of magnitude larger than the glyoxal aerosol sink that we observe in Pasadena. The calculated uptake coefficient in Mexico City, γ, was 4.2 × 10^{-3} (with uncertainty +6 × 10^{-3} and −2 × 10^{-3}) at 11:00 and 2.5 × 10^{-3} (with uncertainty +2 × 10^{-3} and −1 × 10^{-3}) at 15:00 [*Volkamer et al.*, 2007]. For Mexico City, the difference between modeled and measured glyoxal concentrations was 200–600%, leading to an unambiguous determination of heterogeneous loss processes in addition to photolysis and OH reaction [*Volkamer et al.*, 2007]. For the Pasadena field study, we find a difference of 0 to 30% between the MCM model predictions and measurements. The large difference in the fraction of glyoxal production attributable to sinks in addition to OH and photolysis in these two cities may be caused by a number of factors, including the larger available aerosol surface area in Mexico City or differences in aerosol composition between the two cities. The VOC chemistry differs between the two cities as well. Glyoxal production in Mexico City is dominated

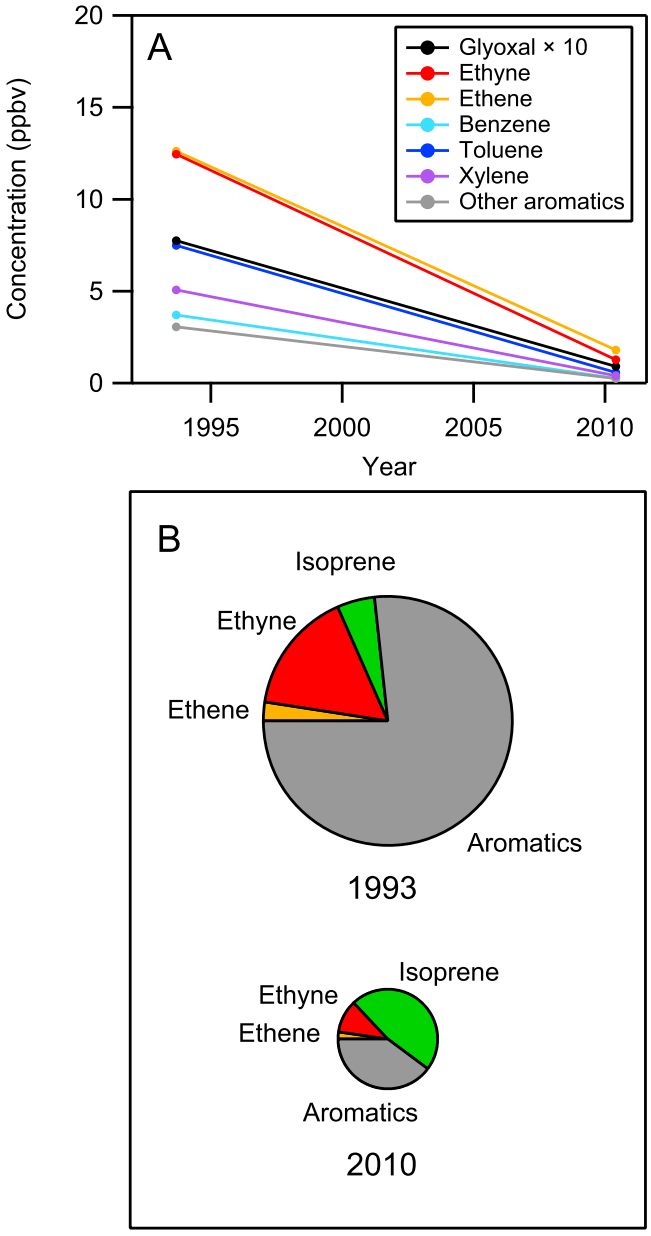

Figure 7. (a) Average VOC concentrations reported during 8–9 September 1993 for five locations in Los Angeles [*Grosjean et al.*, 1996; *Fraser et al.*, 1997, 1998] and average VOC concentrations for Pasadena during 15 May to 16 June 2010. VOCs plotted are glyoxal; ethyne; ethene; benzene; toluene; xylenes; and other aromatics. (b) Steady state glyoxal production calculated for average VOC concentrations in Figure 7a. The area of the pie charts are proportional to the total glyoxal production rates, which were 670 pptv h^{-1} in 1993 and 100 pptv h^{-1} in 2010.

by anthropogenic species, including aromatics, while biogenic species play an important role at the Pasadena field site. Differences in the analysis between the two cities may indicate a lack of understanding in VOC oxidation mechanisms. Further field or laboratory work will be required to understand the factors that control the heterogeneous chemistry of glyoxal.

3.6. Historical Trends in Glyoxal and VOC Precursor Concentrations

[55] The measurements acquired during the CalNex field campaign can be compared to prior measurements in Los Angeles. A comprehensive set of VOC measurements was acquired during 8–9 September 1993 at five sites in the Los Angeles area with the goal of providing data to evaluate air quality models. The locations were Long Beach, downtown Los Angeles, Azusa, Claremont, and San Nicolas Island. These measurements included: C_1–C_{14} carbonyls, glyoxal, and methyl glyoxal, [*Grosjean et al.*, 1996]; C_6–C_{22} nonpolar and semipolar aromatics [*Fraser et al.*, 1998]; and C_2–C_{36} non-aromatic hydrocarbons including isoprene [*Fraser et al.*, 1997].

[56] VOC precursor and glyoxal concentrations are shown in Figure 7a. For both data sets, the diurnal average is shown, because no time-resolved data was reported for VOC precursors [*Fraser et al.*, 1997, 1998]. The 1993 measurements were recorded during a September smog episode and are given as the average of five sampling locations, while the CalNex 2010 data were recorded at a single location earlier in the season. Despite the sampling differences between the two data sets, they indicate a large decrease in VOC concentrations that corresponds to successful emission control strategies that have been implemented in the Los Angeles basin. Diurnally averaged glyoxal concentrations have decreased from 775 pptv in 1993 to 91 pptv in 2010.

[57] Glyoxal production was calculated from the diurnally averaged precursor concentrations shown in Figure 7a, using the steady state method described in section 3.3 with an assumed OH concentration of 5×10^6 cm^{-3}. To better represent the daytime production of glyoxal, mid-day isoprene concentrations are shown. Mid-day isoprene concentrations for 1993 were calculated by scaling the reported diurnal average by the measured ratio of mid-day to diurnal average (2.5) for the 2010 Pasadena field site. Figure 7b shows that glyoxal production from known precursors has decreased by 85% from 670 pptv h^{-1} in 1993 to 100 pptv h^{-1} in 2010. Although this comparison relies on limited historical data, it provides insight into long-term air quality trends in Los Angeles. The comparison of the 1993 and 2010 data shows that 1) calculated glyoxal production rates and measured glyoxal concentrations were both much higher in the past; 2) as anthropogenic emissions have decreased, biogenic isoprene emissions have become a larger fraction of the total glyoxal production; and 3) glyoxal's potential mass available to secondary organic aerosol has decreased over time.

4. Conclusions

[58] We measured glyoxal during summer 2010 at the CalNex ground site in Pasadena, California. The glyoxal measurements were co-located with an extensive suite of trace gas, photolysis, aerosol size distribution and composition, meteorology, and ceilometer data. Additional coincident data by the NOAA WP-3 aircraft and RV Atlantis allowed boundary conditions to be constrained.

[59] Previous laboratory and field studies have shown that glyoxal contributes to secondary organic aerosol. We analyzed the measurements using three independent methods to calculate the contribution of glyoxal to SOA: 1) steady state analysis; 2) a pseudo-Lagrangian two-dimensional chemical

model; and 3) nighttime loss. The first two methods show that isoprene is the major daytime glyoxal source for the field measurements in Pasadena, contributing more than 60% during clear, mid-day conditions. The two-dimensional chemical model shows that 0–30% of glyoxal production is available for heterogeneous uptake. This result differs from a recent study in Mexico City that reported a much larger discrepancy between glyoxal sources and sinks, implying a much larger secondary organic aerosol source from glyoxal production and loss. The reasons for this difference may include a larger aerosol surface area for heterogeneous reactions in Mexico City, differences in aerosol composition or liquid water content between the two cities that lead to variability in glyoxal heterogeneous chemistry, or differences in the predominant VOC precursors. Further investigation of the role of glyoxal in the ambient atmosphere in different locations and seasons will be of significant interest to understand the reasons underlying this variability.

[60] **Acknowledgments.** J.L.J. and J.A.d.G. thank Jochen Stutz and Jason Surratt for co-organizing the CalNex site in Pasadena. We thank the California Air Resources Board for funding the site, and the California Institute of Technology for hosting it. We thank Nicholas Wagner, William Dubé, and Steve Ciciora for contributing to the design and construction of the IBBCEAS instrument. We thank Eric Williams and Brian Lerner for O_3 and NO_x measurements from the RV Atlantis. We thank Jochen Stutz and Andrew Langford for scientific discussions about spectral fitting. We thank Charles Brock for scientific discussions about aerosol properties. We acknowledge financial support for the IBBCEAS field instrument development from the NOAA Assistant Administrator's 2008 Discretionary Fund. We acknowledge financial support for the field measurements from the NOAA Air Quality and NOAA Climate Research and Modeling programs. P.L.H., M.J.C., and J.L.J. were supported by CARB 08-319 and NOAA NA08OAR4310565.

References

Atkinson, R. (1994), Gas-phase tropospheric chemistry of organic compounds, *J. Phys. Chem. Ref. Data*, *37*, suppl. 2, 197–219.

Atkinson, R. (1997), Gas-phase tropospheric chemistry of volatile organic compounds: 1. Alkanes and alkenes, *J. Phys. Chem. Ref. Data*, *26*(2), 215–290, doi:10.1063/1.556012.

Atkinson, R., et al. (1981), Rate constants for the gas-phase reactions of O_3 with a series of carbonyls at 296 K, *Int. J. Chem. Kinet.*, *13*(11), 1133–1142, doi:10.1002/kin.550131104.

Atkinson, R., et al. (2005), Summary of evaluated kinetic and photochemical data for atmospheric chemistry, IUPAC Subcomm. on Gas Kinet., Data Eval. for Atmos. Chem., Research Triangle Park, N. C.

Atkinson, R., et al. (2006), Evaluated kinetic and photochemical data for atmospheric chemistry: Volume II—Gas phase reactions of organic species, *Atmos. Chem. Phys.*, *6*, 3625–4055, doi:10.5194/acp-6-3625-2006.

Bacher, C., et al. (2001), The atmospheric chemistry of glycolaldehyde, *J. Atmos. Chem.*, *39*(2), 171–189, doi:10.1023/A:1010689706869.

Ban-Weiss, G. A., et al. (2008), Carbonyl and nitrogen dioxide emissions from gasoline- and diesel-powered motor vehicles, *Environ. Sci. Technol.*, *42*(11), 3944–3950, doi:10.1021/es8002487.

Bloss, C., et al. (2005), Development of a detailed chemical mechanism (MCMv3.1) for the atmospheric oxidation of aromatic hydrocarbons, *Atmos. Chem. Phys.*, *5*, 641–664, doi:10.5194/acp-5-641-2005.

Bon, D. M., et al. (2011), Measurements of volatile organic compounds at a suburban ground site (T1) in Mexico City during the MILAGRO 2006 campaign: Measurement comparison, emission ratios, and source attribution, *Atmos. Chem. Phys.*, *11*, 2399–2421, doi:10.5194/acp-11-2399-2011.

Brown, S. S., et al. (2009), Reactive uptake coefficients for N_2O_5 determined from aircraft measurements during the Second Texas Air Quality Study: Comparison to current model parameterizations, *J. Geophys. Res.*, *114*, D00F10, doi:10.1029/2008JD011679.

Calvert, J. G., et al. (2000), *The Mechanisms of Atmospheric Oxidation of the Alkenes*, 552 pp., Oxford Univ. Press, New York.

Carlton, A. G., et al. (2007), Atmospheric oxalic acid and SOA production from glyoxal: Results of aqueous photooxidation experiments, *Atmos. Environ.*, *41*(35), 7588–7602, doi:10.1016/j.atmosenv.2007.05.035.

Colman, J. J., et al. (2001), Description of the analysis of a wide range of volatile organic compounds in whole air samples collected during PEM-Tropics A and B, *Anal. Chem.*, *73*(15), 3723–3731, doi:10.1021/ac010027g.

Corrigan, A. L., et al. (2008), Uptake of glyoxal by organic and inorganic aerosol, *Environ. Sci. Technol.*, *42*(12), 4428–4433, doi:10.1021/es7032394.

DeCarlo, P. F., et al. (2006), Field-deployable, high-resolution, time-of-flight aerosol mass spectrometer, *Anal. Chem.*, *78*(24), 8281–8289, doi:10.1021/ac061249n.

de Gouw, J. A., et al. (2005), Budget of organic carbon in a polluted atmosphere: Results from the New England Air Quality Study in 2002, *J. Geophys. Res.*, *110*(D16), D16305, doi:10.1029/2004JD005623.

De Haan, D. O., et al. (2009a), Secondary organic aerosol forming reactions of glyoxal with amino acids, *Environ. Sci. Technol.*, *43*(8), 2818–2824, doi:10.1021/es803534f.

De Haan, D. O., M. A. Tolbert, and J. L. Jimenez (2009b), Atmospheric condensed-phase reactions of glyoxal with methylamine, *Geophys. Res. Lett.*, *36*, L11819, doi:10.1029/2009GL037441.

Dube, W. P., et al. (2006), Aircraft instrument for simultaneous, in situ measurement of NO_3 and N_2O_5 via pulsed cavity ring-down spectroscopy, *Rev. Sci. Instrum.*, *77*(3), doi:10.1063/1.2176058.

Dusanter, S., et al. (2009), Measurements of OH and HO_2 concentrations during the MCMA-2006 field campaign—Part 1: Deployment of the Indiana University laser-induced fluorescence instrument, *Atmos. Chem. Phys.*, *9*(5), 1665–1685, doi:10.5194/acp-9-1665-2009.

Dzepina, K., et al. (2009), Evaluation of recently proposed secondary organic aerosol models for a case study in Mexico City, *Atmos. Chem. Phys.*, *9*(15), 5681–5709, doi:10.5194/acp-9-5681-2009.

Dzepina, K., et al. (2011), Modeling the multiday evolution and aging of secondary organic aerosol during MILAGRO 2006, *Environ. Sci. Technol.*, *45*(8), 3496–3503, doi:10.1021/es103186f.

Ervens, B., and R. Volkamer (2010), Glyoxal processing by aerosol multiphase chemistry: Towards a kinetic modeling framework of secondary organic aerosol formation in aqueous particles, *Atmos. Chem. Phys.*, *10*(17), 8219–8244, doi:10.5194/acp-10-8219-2010.

Feierabend, K. J., et al. (2008), Rate coefficients for the OH+HC(O)C(O)H (glyoxal) reaction between 210 and 390, *J. Phys. Chem. A*, *112*(1), 73–82, doi:10.1021/jp0768571.

Feierabend, K. J., et al. (2009), HCO quantum yields in the photolysis of HC(O)C(O)H (glyoxal) between 290 and 420 nm, *J. Phys. Chem. A*, *113*(27), 7784–7794, doi:10.1021/jp9033003.

Fraser, M. P., et al. (1997), Air quality model evaluation data for organics. 4. C_2–C_{36} non-aromatic hydrocarbons, *Environ. Sci. Technol.*, *31*(8), 2356–2367, doi:10.1021/es960980g.

Fraser, M. P., et al. (1998), Air quality model evaluation data for organics. 5. C_6–C_{22} nonpolar and semipolar aromatic compounds, *Environ. Sci. Technol.*, *32*(12), 1760–1770, doi:10.1021/es970349v.

Fu, T. M., D. J. Jacob, F. Wittrock, J. P. Burrows, M. Vrekoussis, and D. K. Henze (2008), Global budgets of atmospheric glyoxal and methylglyoxal, and implications for formation of secondary organic aerosols, *J. Geophys. Res.*, *113*, D15303, doi:10.1029/2007JD009505.

Fuchs, H., et al. (2009), A sensitive and versatile detector for atmospheric NO_2 and NO_x based on blue diode laser cavity ring-down spectroscopy, *Environ. Sci. Technol.*, *43*(20), 7831–7836, doi:10.1021/es902067h.

Fuchs, N. A., and A. G. Sutugin (1971), Highly dispersed aerosol, in *Topics in Current Aerosol Research*, edited by G. M. Hidy and J. R. Brock, pp. 1–60, Pergamon, New York.

Fung, K., and D. Grosjean (1981), Determination of nanogram amounts of carbonyls as 2,4-dinitrophenylhydrazones by high-performance liquid-chromatography, *Anal. Chem.*, *53*(2), 168–171, doi:10.1021/ac00225a009.

Galloway, M. M. (2011), Yields of oxidized volatile organic compounds during the OH radical initiated oxidation of isoprene, methyl vinyl ketone, and methacrolein under high-NO_x conditions, *Atmos. Chem. Phys. Discuss.*, *11*, 10,693–10,720, doi:10.5194/acpd-11-10693-2011.

Galloway, M. M., et al. (2009), Glyoxal uptake on ammonium sulphate seed aerosol: Reaction products and reversibility of uptake under dark and irradiated conditions, *Atmos. Chem. Phys.*, *9*(10), 3331–3345, doi:10.5194/acp-9-3331-2009.

Gilman, J. B., et al. (2010), Ozone variability and halogen oxidation within the Arctic and sub-Arctic springtime boundary layer, *Atmos. Chem. Phys.*, *10*(21), 10,223–10,236, doi:10.5194/acp-10-10223-2010.

Grosjean, E., et al. (1996), Air quality model evaluation data for organics. 2. C_1–C_{14} carbonyls in Los Angeles air, *Environ. Sci. Technol.*, *30*(9), 2687–2703, doi:10.1021/es950758w.

Guenther, A. B., et al. (1993), Isoprene and monoterpene emission rate variability: Model evaluations and sensitivity analyses, *J. Geophys. Res.*, *98*(D7), 12,609–12,617, doi:10.1029/93JD00527.

Guenther, A., et al. (1994), Natural volatile organic compound emission rate estimates for United States woodland landscapes, *Atmos. Environ.*, *28*(6), 1197–1210, doi:10.1016/1352-2310(94)90297-6.

Hastings, W. P., et al. (2005), Secondary organic aerosol formation by glyoxal hydration and oligomer formation: Humidity effects and equilibrium shifts during analysis, *Environ. Sci. Technol.*, *39*(22), 8728–8735, doi:10.1021/es0504461.

Heald, C. L., D. J. Jacob, R. J. Park, L. M. Russell, B. J. Huebert, J. H. Seinfeld, H. Liao, and R. J. Weber (2005), A large organic aerosol source in the free troposphere missing from current models, *Geophys. Res. Lett.*, *32*, L18809, doi:10.1029/2005GL023831.

Huisman, A. J., et al. (2008), Laser-induced phosphorescence for the in situ detection of glyoxal at part per trillion mixing ratios, *Anal. Chem.*, *80*(15), 5884–5891, doi:10.1021/ac800407b.

Huisman, A. J., et al. (2011), Photochemical modeling of glyoxal at a rural site: Observations and analysis from BEARPEX 2007, *Atmos. Chem. Phys. Discuss.*, *11*, 13,655–13,691, doi:10.5194/acpd-11-13655-2011.

Igawa, M., et al. (1989), Analysis of aldehydes in cloud samples and fog-water samples by HPLC with a postcolumn reaction detector, *Environ. Sci. Technol.*, *23*(5), 556–561, doi:10.1021/es00063a007.

Ip, H. S. S., X. H. H. Huang, and J. Z. Yu (2009), Effective Henry's law constants of glyoxal, glyoxylic acid, and glycolic acid, *Geophys. Res. Lett.*, *36*, L01802, doi:10.1029/2008GL036212.

Jang, M. S., and R. M. Kamens (2001), Atmospheric secondary aerosol formation by heterogeneous reactions of aldehydes in the presence of a sulfuric acid aerosol catalyst, *Environ. Sci. Technol.*, *35*(24), 4758–4766, doi:10.1021/es010790s.

Jang, M. S., et al. (2002), Heterogeneous atmospheric aerosol production by acid-catalyzed particle-phase reactions, *Science*, *298*(5594), 814–817, doi:10.1126/science.1075798.

Jenkin, M. E., et al. (2003), Protocol for the development of the Master Chemical Mechanism, MCM v3 (Part B): Tropospheric degradation of aromatic volatile organic compounds, *Atmos. Chem. Phys.*, *3*, 181–193, doi:10.5194/acp-3-181-2003.

Jimenez, J. L., et al. (2009), Evolution of organic aerosols in the atmosphere, *Science*, *326*(5959), 1525–1529, doi:10.1126/science.1180353.

Johnson, D., et al. (2006), Simulating regional scale secondary organic aerosol formation during the TORCH 2003 campaign in the southern UK, *Atmos. Chem. Phys.*, *6*, 403–418, doi:10.5194/acp-6-403-2006.

Kanakidou, M., et al. (2005), Organic aerosol and global climate modelling: A review, *Atmos. Chem. Phys.*, *5*, 1053–1123, doi:10.5194/acp-5-1053-2005.

Karl, T., M. Potosnak, A. Guenther, D. Clark, J. Walker, J. D. Herrick, and C. Geron (2004), Exchange processes of volatile organic compounds above a tropical rain forest: Implications for modeling tropospheric chemistry above dense vegetation, *J. Geophys. Res.*, *109*, D18306, doi:10.1029/2004JD004738.

Karl, T., et al. (2010), Efficient atmospheric cleansing of oxidized organic trace gases by vegetation, *Science*, *330*(6005), 816–819, doi:10.1126/science.1192534.

Kraus, S. G. (2006), DOASIS: A framework design for DOAS, Ph.D. dissertation, Univ. of Mannheim, Mannheim, Germany.

Kroll, J. H., and J. H. Seinfeld (2005), Representation of secondary organic aerosol laboratory chamber data for the interpretation of mechanisms of particle growth, *Environ. Sci. Technol.*, *39*(11), 4159–4165, doi:10.1021/es048292h.

Kroll, J. H., N. L. Ng, S. M. Murphy, V. Varutbangkul, R. C. Flagan, and J. H. Seinfeld (2005), Chamber studies of secondary organic aerosol growth by reactive uptake of simple carbonyl compounds, *J. Geophys. Res.*, *110*, D23207, doi:10.1029/2005JD006004.

Lewis, A. C., et al. (2005), Sources and sinks of acetone, methanol, and acetaldehyde in North Atlantic marine air, *Atmos. Chem. Phys.*, *5*, 1963–1974, doi:10.5194/acp-5-1963-2005.

Liggio, J., et al. (2005a), Heterogeneous reactions of glyoxal on particulate matter: Identification of acetals and sulfate esters, *Environ. Sci. Technol.*, *39*(6), 1532–1541, doi:10.1021/es048375y.

Liggio, J., S.-M. Li, and R. McLaren (2005b), Reactive uptake of glyoxal by particulate matter, *J. Geophys. Res.*, *110*, D10304, doi:10.1029/2004JD005113.

Millet, D. B., et al. (2010), Global atmospheric budget of acetaldehyde: 3-D model analysis and constraints from in-situ and satellite observations, *Atmos. Chem. Phys.*, *10*(7), 3405–3425, doi:10.5194/acp-10-3405-2010.

Munkel, C., et al. (2007), Retrieval of mixing height and dust concentration with lidar ceilometer, *Boundary Layer Meteorol.*, *124*(1), 117–128, doi:10.1007/s10546-006-9103-3.

Naik, V., et al. (2010), Observational constraints on the global atmospheric budget of ethanol, *Atmos. Chem. Phys.*, *10*(12), 5361–5370, doi:10.5194/acp-10-5361-2010.

Pankow, J. F. (1994a), An absorption model of the gas/aerosol partitioning involved in the formation of secondary organic aerosol, *Atmos. Environ.*, *28*(2), 189–193, doi:10.1016/1352-2310(94)90094-9.

Pankow, J. F. (1994b), An absorption model of gas/particle partitioning of organic compounds in the atmosphere, *Atmos. Environ.*, *28*(2), 185–188, doi:10.1016/1352-2310(94)90093-0.

Pilling, M. J., and P. W. Seakins (1995), *Reaction Kinetics*, 305 pp., Oxford Univ. Press, Oxford, U. K.

Plum, C. N., et al. (1983), OH radical rate constants and photolysis rates of α-dicarbonyls, *Environ. Sci. Technol.*, *17*(8), 479–484, doi:10.1021/es00114a008.

Pollack, I. B., et al. (2011), Evaluation of ultraviolet light-emitting diodes for detection of atmospheric NO_2 by photolysis-chemiluminescence, *J. Atmos. Chem.*, *65*, 111–125, doi:10.1007/s10874-011-9184-3.

Robinson, A. L., et al. (2007), Rethinking organic aerosols: Semivolatile emissions and photochemical aging, *Science*, *315*(5816), 1259–1262, doi:10.1126/science.1133061.

Ryerson, T. B., et al. (1998), Emissions lifetimes and ozone formation in power plant plumes, *J. Geophys. Res.*, *103*(D17), 22,569–22,583, doi:10.1029/98JD01620.

Ryerson, T. B., E. J. Williams, and F. C. Fehsenfeld (2000), An efficient photolysis system for fast-response NO_2 measurements, *J. Geophys. Res.*, *105*(D21), 26,447–26,461, doi:10.1029/2000JD900389.

Sander, S. P., et al. (2006), Chemical kinetics and photochemical data for use in atmospheric studies, Jet Propul. Lab., Pasadena, Calif.

Saunders, S. M., et al. (2003), Protocol for the development of the Master Chemical Mechanism, MCM v3 (Part A): Tropospheric degradation of non-aromatic volatile organic compounds, *Atmos. Chem. Phys.*, *3*, 161–180.

Shapiro, E. L., et al. (2009), Light-absorbing secondary organic material formed by glyoxal in aqueous aerosol mimics, *Atmos. Chem. Phys.*, *9*(7), 2289–2300, doi:10.5194/acp-9-2289-2009.

Shetter, R. E., and M. Muller (1999), Photolysis frequency measurements using actinic flux spectroradiometry during the PEM-Tropics mission: Instrumentation description and some results, *J. Geophys. Res.*, *104*(D5), 5647–5661, doi:10.1029/98JD01381.

Sinreich, R., et al. (2007), MAX-DOAS detection of glyoxal during ICARTT 2004, *Atmos. Chem. Phys.*, *7*, 1293–1303, doi:10.5194/acp-7-1293-2007.

Skamarock, W. C., et al. (2008), A description of the Advanced Research WRF version 3, *Tech. Note NCAR/TN-475+STR*, Mesoscale and Microscale Meteorol. Div., Natl. Cent. for Atmos. Res., Boulder, Colo.

Spaulding, R. S., et al. (2002), Optimization of a mist chamber (cofer scrubber) for sampling water-soluble organics in air, *Environ. Sci. Technol.*, *36*(8), 1798–1808, doi:10.1021/es011189x.

Steinberg, S., et al. (1985), The determination of alpha-keto acids and oxalic-acid in rain, fog and mist by HPLC, *Int. J. Environ. Anal. Chem.*, *19*(4), 251–260, doi:10.1080/03067318508077036.

Tan, Y., et al. (2009), Effects of precursor concentration and acidic sulfate in aqueous glyoxal-OH radical oxidation and implications for secondary organic aerosol, *Environ. Sci. Technol.*, *43*(21), 8105–8112, doi:10.1021/es901742f.

Thalman, R., and R. Volkamer (2010), Inherent calibration of a blue LED-CE-DOAS instrument to measure iodine oxide, glyoxal, methyl glyoxal, nitrogen dioxide, water vapour and aerosol extinction in open cavity mode, *Atmos. Meas. Tech.*, *3*(6), 1797–1814, doi:10.5194/amt-3-1797-2010.

U. S. Census Bureau (2006), Annual estimates of the population of metropolitan and micropolitan statistical areas: April 1, 2000 to July 1, 2007 (CBSA-EST2007-01), Washington, D. C.

Vandaele, A. C., et al. (1998), Measurements of the NO_2 absorption cross-section from 42000 cm^{-1} to 10000 cm^{-1} (238–1000 nm) at 220 K and 294 K, *J. Quant. Spectrosc. Radiat. Transfer*, *59*(3–5), 171–184, doi:10.1016/S0022-4073(97)00168-4.

Volkamer, R., L. T. Molina, M. J. Molina, T. Shirley, and W. H. Brune (2005a), DOAS measurement of glyoxal as an indicator for fast VOC chemistry in urban air, *Geophys. Res. Lett.*, *32*, L08806, doi:10.1029/2005GL022616.

Volkamer, R., et al. (2005b), High-resolution absorption cross-section of glyoxal in the UV-VIS and IR spectral ranges, *J. Photochem. Photobiol. A*, *172*(1), 35–46, doi:10.1016/j.jphotochem.2004.11.011.

Volkamer, R., et al. (2006a), Remote sensing of glyoxal by differential optical absorption spectroscopy (DOAS): Advancements in simulation chamber and field experiments, in *Environmental Simulation Chambers: Application to Atmospheric Chemical Processes*, edited by I. Barnes and K. J. Rudzinski, pp. 129–141, Kluwer Acad., Dordrecht, Netherlands, doi:10.1007/1-4020-4232-9_10.

Volkamer, R., J. L. Jimenez, F. San Martini, K. Dzepina, Q. Zhang, D. Salcedo, L. T. Molina, D. R. Worsnop, and M. J. Molina (2006b),

Secondary organic aerosol formation from anthropogenic air pollution: Rapid and higher than expected, *Geophys. Res. Lett.*, *33*, L17811, doi:10.1029/2006GL026899.

Volkamer, R., F. San Martini, L. T. Molina, D. Salcedo, J. L. Jimenez, and M. J. Molina (2007), A missing sink for gas-phase glyoxal in Mexico City: Formation of secondary organic aerosol, *Geophys. Res. Lett.*, *34*, L19807, doi:10.1029/2007GL030752.

Volkamer, R., et al. (2009), Secondary organic aerosol formation from acetylene (C_2H_2): Seed effect on SOA yields due to organic photochemistry in the aerosol aqueous phase, *Atmos. Chem. Phys.*, *9*(6), 1907–1928, doi:10.5194/acp-9-1907-2009.

Warneke, C., S. L. Luxembourg, J. A. de Gouw, H. J. I. Rinne, A. B. Guenther, and R. Fall (2002), Disjunct eddy covariance measurements of oxygenated volatile organic compounds fluxes from an alfalfa field before and after cutting, *J. Geophys. Res.*, *107*(D8), 4067, doi:10.1029/2001JD000594.

Warneke, C., et al. (2007), Determination of urban volatile organic compound emission ratios and comparison with an emissions database, *J. Geophys. Res.*, *112*, D10S47, doi:10.1029/2006JD007930.

Washenfelder, R. A., et al. (2008), Measurement of glyoxal using an incoherent broadband cavity enhanced absorption spectrometer, *Atmos. Chem. Phys.*, *8*(24), 7779–7793, doi:10.5194/acp-8-7779-2008.

Williams, E. J., B. M. Lerner, P. C. Murphy, S. C. Herndon, and M. S. Zahniser (2009), Emissions of NO_x, SO_2, CO, and HCHO from commercial marine shipping during Texas Air Quality Study (TexAQS) 2006, *J. Geophys. Res.*, *114*, D21306, doi:10.1029/2009JD012094.

Zhang, Q., et al. (2007), Ubiquity and dominance of oxygenated species in organic aerosols in anthropogenically-influenced Northern Hemisphere midlatitudes, *Geophys. Res. Lett.*, *34*, L13801, doi:10.1029/2007GL029979.

Zhou, X. L., and K. Mopper (1990), Apparent partition coefficients of 15 carbonyl compounds between air and seawater and between air and freshwater; implications for air sea exchange, *Environ. Sci. Technol.*, *24*(12), 1864–1869, doi:10.1021/es00082a013.

W. M. Angevine, D. M. Bon, M. J. Cubison, J. A. de Gouw, J. B. Gilman, M. Graus, P. L. Hayes, J. L. Jimenez, W. C. Kuster, I. B. Pollack, H. Stark, R. A. Washenfelder, and C. J. Young, Cooperative Institute for Research in Environmental Sciences, University of Colorado at Boulder, 216 UCB, Boulder, CO 80309, USA. (rebecca.washenfelder@noaa.gov)

E. L. Atlas, Division of Marine and Atmospheric Chemistry, University of Miami, Miami, FL 33149, USA.

D. R. Blake, Department of Chemistry, University of California, 570 Rowland Hall, Irvine, CA 92697, USA.

S. S. Brown, T. B. Ryerson, and M. K. Trainer, Chemical Sciences Division, Earth System Research Laboratory, National Oceanic and Atmospheric Administration, 325 Broadway, Boulder, CO 80305, USA.

S. Dusanter, S. Griffith, and P. S. Stevens, Center for Research in Environmental Science, School of Public and Environmental Affairs, Indiana University, Bloomington, IN 47405, USA.

J. Flynn, N. Grossberg, and B. L. Lefer, Department of Earth and Atmospheric Sciences, University of Houston, Houston, TX 77204, USA.